Spiropiperidine-Based Oligomycin-Analog Ligands To Counteract the Ischemia−Reperfusion Injury in a Renal Cell Model

Giulia Turrin,[§] Ettore Lo Cascio,[§] Noah Giacon, Anna Fantinati, Virginia Cristofori, Davide Illuminati, Delia Preti, Giampaolo Morciano, Paolo Pinton, Esther Densu Agyapong, Claudio Trapella,* and Alessandro Arcovito*

Cite This: *J. Med. Chem.* 2024, 67, 586−602

Read Online

ACCESS | Metrics & More | Article Recommendations | Supporting Information

ABSTRACT: Finding a therapy for ischemia−reperfusion injury, which consists of cell death following restoration of blood flowing into the artery affected by ischemia, is a strong medical need. Nowadays, only the use of broad-spectrum molecular therapies has demonstrated a partial efficacy in protecting the organs following reperfusion, while randomized clinical trials focused on more specific drug targets have failed. In order to overcome this problem, we applied a combination of molecular modeling and chemical synthesis to identify novel spiropiperidine-based structures active in mitochondrial permeability transition pore opening inhibition as a key process to enhance cell survival after blood flow restoration. Our results were confirmed by biological assay on an in vitro cell model on HeLa and human renal proximal tubular epithelial cells and pave the way to further investigation on an in vivo model system.
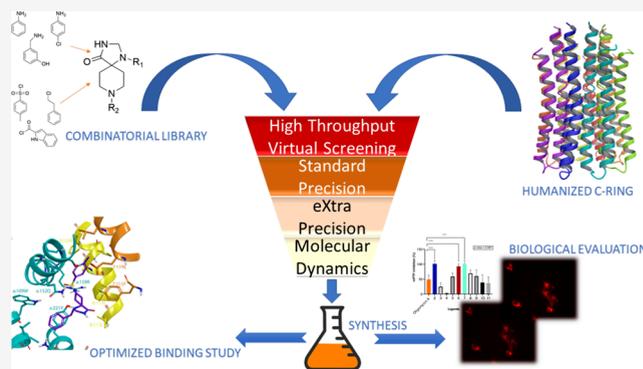
INTRODUCTION

Programmed cell death is an evolutionarily conserved physiological event, essential for intrauterine and postembryonic development and for tissue homeostasis, through the elimination of damaged cells that otherwise would lead to numerous pathological events.[1] Conversely, in humans, excessive apoptosis can lead to a long list of pathological dysfunctions, such as cardiovascular, neurological, and nephrological disorders. There are several types of programmed cell death, including apoptosis mediated by the transition of mitochondrial permeability,[2] which results in an increase in the permeability of the inner mitochondrial membrane (IMM, usually highly impermeable) with consequent osmotic influx of solutes in the mitochondrial matrix and loss of the structural and functional characteristics of the mitochondria involved.[3] The mitochondrial permeability transition (MPT) state is mediated by the opening of a channel called the mitochondrial permeability transition pore (mPTP), a multiprotein platform consisting of proteins that physically form a pore inside the IMM with negative and positive modulators that contribute to its functional state and its formation mechanism.[4] Among the conditions that favor the opening of mPTP are the increase in the concentration of calcium ions (Ca^{2+}) in the mitochondrial matrix, restoration of pH levels, oxidative stress, and the presence of phosphates, all events that occur in response to injuries due to an ischemia−reperfusion condition (I/R).[4,5] Although many of the components and

modulators of mPTP have been discovered in recent years, the proteins that delimit the channel are still the subject of intense study. Among the known mPTP modulators are different types of molecules; to cite a few examples, cyclophilin D (CypD) is a soluble protein of the mitochondrial matrix,[6] and its stable depletion has been shown to lead to a protective and desensitization behavior of MPT. Regarding the class of small molecules, triazoles and isoxazoles have been also investigated as potential compounds modulating mPTP opening by targeting the F_1 of ATPase;[7,8] meanwhile, urea-based compounds have been shown to inhibit mPTP opening by interacting with the F_O domain.[7] In two recent studies,[9,10] experimental evidence is provided showing that subunit C of the F_1/F_O-ATP synthase plays a fundamental role in the activity and formation of mPTP, demonstrating in particularly a strong correlation between the expression of the C subunit and the functional state of mPTP. In fact, the depletion of this protein leads to a reduction of the channel opening in response to oxidative stress or calcium-induced stress, while its overexpression stimulates the opening.
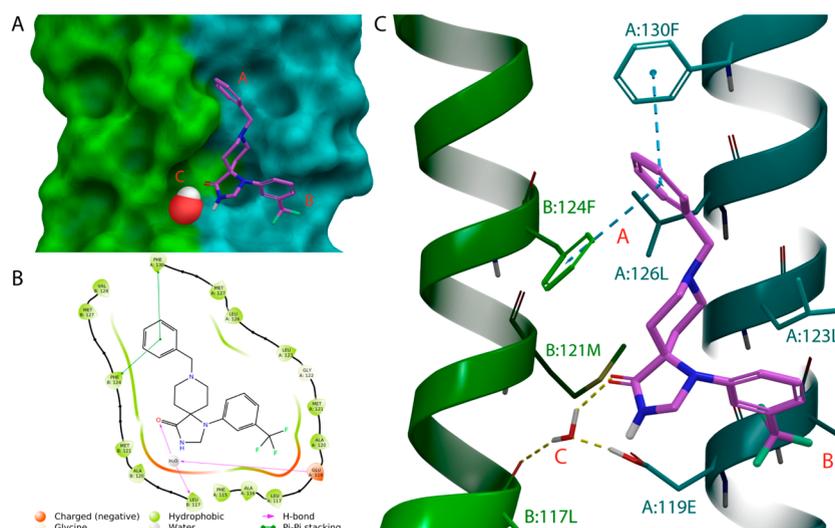
Figure 1. C-subunits–compound **1** complex binding mode. (A) Binding pose of compound **1** against humanized C-ring subunits shown as a colored surface (chain A in cyan and chain B in green, compound **1** in purple) obtained via homology modeling. (B) Ligand interaction diagram of the binding mode. (C) Zoomed-in view of the complex. Yellow dotted lines represent hydrogen bonds; blue dotted lines show π-stacking interactions.

However, it is worth noting that the role of the C subunit of F_1/F_O-ATP synthase as a key element of the mPTP is still under debate. Recent experiments have provided evidence suggesting that mPTP may persist even after the knockout of the C subunit,[11] even if, in further study, it was seen that this pore has lower conductance compared to the mPTP containing the C subunits.[12] Furthermore, it has been demonstrated that the C ring, in its native state, does not function as a pore due to the presence of a lipid plug in the center.[13]

Therefore, the opening of the mPTP is a multistep process involving (i) the dissociation of F_1/F_O-ATP synthase dimers and (ii) an appropriate conformation of the protein ring consisting of multiple C subunits once these dimers dissociated. Other groups, such as Alavian's, Azarashvili's, and collaborators, have independently confirmed these observations by adding important base notions on the properties of the channel[14] and the relative phosphorylation state.[15] The molecular organization of the C subunit in an annular structure (C ring) in IMM causes this to be identified as a key component in the pore assembly process[16] as well as a promising therapeutic target for the pharmacological treatment of programmed cell death.[17,18] Although numerous efforts have been made to synthesize and test new inhibitors of the mPTP opening,[19,20] to the best of our knowledge, only a few structures have been identified to date showing specificity of interaction with the C subunit.[7,16] Indeed, not one reached clinical usage for cardioprotective or nephroprotective purposes for the treatment of ischemia–reperfusion injury (IRI), which consists of cell death following restoration of blood flowing into the artery affected by ischemia.[18] To date, only the use of broad-spectrum molecular therapies has demonstrated useful efficacy in protecting the organs following reperfusion, while randomized clinical trials focused on more specific drug targets have failed. Therefore, the clinical need for a new pharmacological and/or therapeutic approach for the treatment of pathologies deriving from damage related to reperfusion is still pressing.

■ RESULTS AND DISCUSSION

Spiropiperidine Binding Site Characterization. Given the growing development of computational chemistry methods in the field of molecular modeling, the binding site of the ATP synthase C ring has been characterized to investigate how the biological system interacts with spiropiperidine-based oligomycin-analog ligands.[21] The C ring is a transmembrane homomeric complex composed by 8–14 subunits. In humans, each subunit consists of 136 amino acids, of which 76 are part of the transmembrane portion having a helix–loop–helix structure. As a starting point for the in silico study, the X-ray crystal of the C ring cocrystallized with oligomycin A was used (PDB ID: 4F4S).[22] Unfortunately, the reported C ring belongs to the yeast mitochondrial ATP synthase which presents some differences in the amino acidic sequence compared to the human one.

So, the protein was "humanized" via homology modeling using the human c-subunit amino acid sequence extracted from Uniprot[23] (code: P05496) before proceeding with the ligand-binding study (see Figure S1).

To investigate the binding mode of the spiropiperidine derivatives, we selected the oligomycin A binding site as a hot spot and chose 8-benzyl-1-(3-(trifluoromethyl)phenyl)-1,3,8-triazaspiro[4.5]decan-4-one (compound **1**, Figure 1) as a molecular probe since it is the most powerful among the inhibitors tested so far with an mPTP-opening inhibition of 60%.[21] Successively, the induced fit docking (IFD) protocol was pursued to identify the interactions useful for inhibiting the mPTP opening, and the results, shown in Figure 1A and 1C, clearly defined three pockets close to the interface between two consecutive subunits as the main structural determinants able to trap possible lead compounds: Pockets A, B, and C.

Pocket A (identified by the following residues A:124F; A:127M; B:130F; B:127M; B:126L) binds the ligand with hydrophobic and π-stacking interactions established between B:130F, A:124F, and the benzyl moiety (in position 8) of the ligand. The conformational arrangement of the residues characterizing this pocket could host more hindered and complex aromatic structures, thus suggesting that a larger moiety of the ligand in this specific position could increase the interaction with the two aromatic residues, thus enhancing the binding affinity.

Pocket B (identified by the following residues B:123L; B:120A; B:116A; B:115F) interacts with the ligand with

hydrophobic contacts, mainly with B:123L, properly orienting the imidazolinone head of the ligand toward the following polar pocket C.

Pocket C contains B:119E which interacts with the carbonyl group of the ligand in position 4 through a hydrogen-bond interaction mediated by a bridging water molecule, thus corresponding to a possible structural element able to specifically set the spiropiperidine moiety in the right orientation to trap it in the desired A and B hydrophobic pockets.

Drug Design and Screening. According to previous results, as a scaffold for a set of novel compounds able to selectively bind the C ring, 1,3,8-triazaspiro[4.5]decan-4-one (spiropiperidine) was used. In order to create the database, a large subset of structures has been retrieved from ZINC15,[24] considering as chemical entities to use as building blocks those previously identified based on the reaction used for the synthesis of spiropiperidine derivatives[21] and detailed below.

The building of the compound library and the screening procedure are schematically represented in Figure 2. Briefly, we have maintained for all of the structures a common

spiropiperidinic scaffold and inserted different substituents both in positions 1 (in Figure 2 generally described as R_1) and 8 (in Figure 2 referred as R_2). Specifically, as building blocks for R_1, which will undergo Strecker reaction, anilines and benzylamines were selected (6755 reactants), while as building blocks for the R_2 group, alkyl, sulfonyl, and acyl halides with an aromatic moiety (phenyl, benzofuranyl, indolyl, imidazolyl, etc.) were chosen (total of 690 reactants). The aromatic ring was necessary to favor the desired $\pi-\pi$ interaction with the two phenylalanines in pocket A. Combining these fragments combinatorially to our spiropiperidine scaffold, 4 660 950 compounds were generated.

In order to shrink this pool, the database was prefiltered as follows. Physical descriptors have been calculated for each molecule by using the QikProp program (Schrödinger) and thus filtered using Lipinski's rule of five and PAINS.[25] The obtained refined library was subsequently subjected to 3 different and gradually more strict docking protocols using as the receptor the previously obtained binding complex. All docking procedures were performed with Glide[26] (Schrödinger).

As a first step, the database was skimmed via a high-throughput virtual screening (HTVS) protocol. Then, the first 10% of molecules selected with the highest docking scores underwent a standard precision (SP) docking procedure, and successively, only the best 10% were docked for the last time using the extra precision (XP) docking procedure.

The obtained poses were further filtered according to the two structural determinants selected during the characterization of the binding site as follows: (1) measuring the distance between the ligands and the two phenylalanines (F124 and F130), hence eliminating the ligands not interacting with these residues; (2) verifying the presence of a water bridge with E119 (taking inspiration from the oligomycin A behavior) and excluding those ligands missing that specific interaction as a possible key element for the correct orientation of the spiropiperidine compounds. These combined efforts led to narrowing the ligands to 100 candidates.

The next step was performed measuring the ligand binding stability by means of 50 ns long molecular dynamics (MD) simulations using the GROMACS engine.[27] All trajectories have been analyzed calculating the number of contacts between the ligands and the protein and compared to oligomycin A, used as reference. Those compounds which could interact more efficiently with the proteins than the reference, especially with E119, F130, F124, and L123, have been selected and are shown in Figure 3.

They can be divided in three families according to the substituent in position 1.

- Compounds **2**–**5** are derived from aniline.
- Compounds **6**–**8** are derived from benzylamine.
- Compounds **9**–**11** correspond to *m*-hydroxy benzylamine derivatives.

All of the compounds of interest have been synthesized, and their biological activity was tested using two different test and cellular lines (described in detail below).

Synthesis of Spiropiperidine Derivatives 2−11. For the synthesis of compounds **2**−**11**, we were initially inspired by the synthetic route previously developed by our group.[21] Subsequently, we modified the synthesis to achieve the compounds of interest.

As a result, we obtained a library of molecules sharing the 1,3,8-triazaspiro-decan-4-one core but differently substituted in
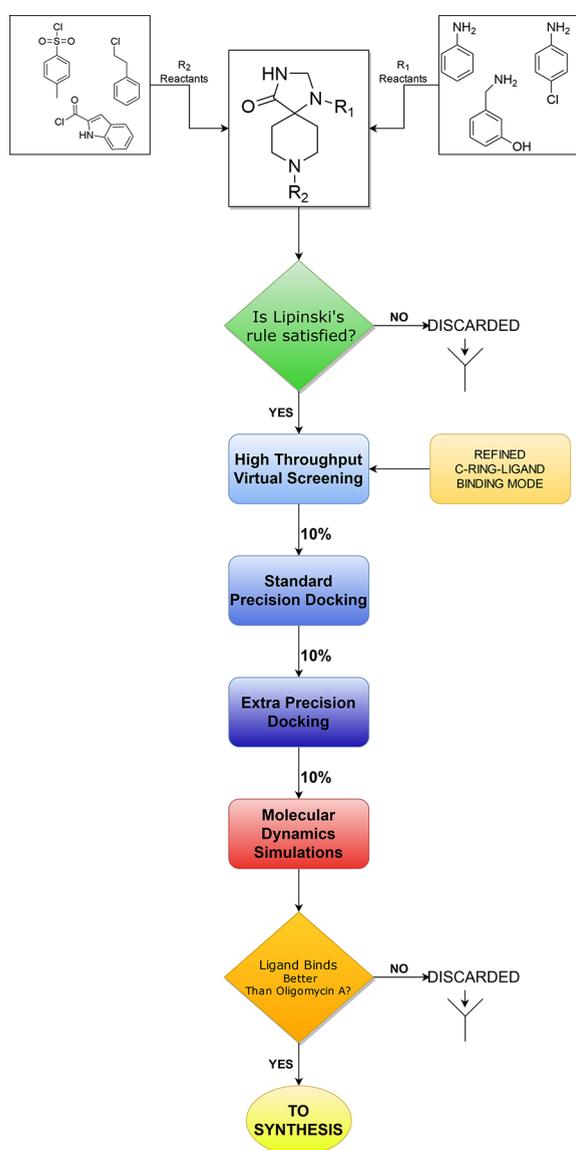

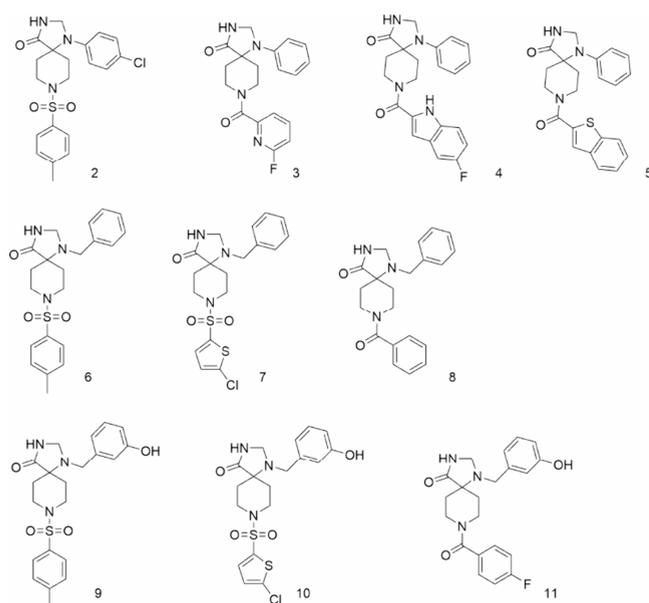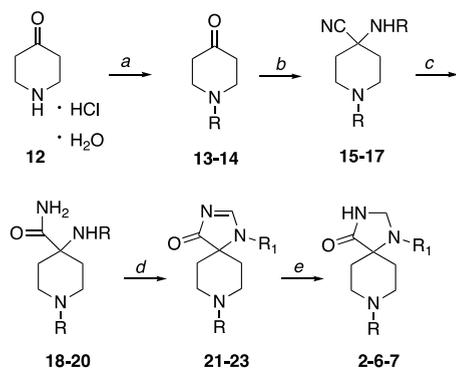**Figure 2.** Schematic representation of the virtual screening protocol.

Figure 3. Compounds selected to be synthesized as a result of the in silico virtual screening.

both the N_1 and the N_8 positions. In particular, as described in Scheme 1, derivatives **2**, **6**, and **7** were obtained from an

Scheme 1. Synthesis of Compounds 2, 6, and 7[a]

[a]Reaction conditions. (*a*) R-SO$_2$Cl, Na$_2$CO$_3$, H$_2$O/diox, rt, 18 h. (*b*) TMSCN, R$_1$NH$_2$, AcOH, rt, 2 h. (*c*) H$_2$SO$_4$ conc., rt, 18 h. (*d*) DMF/DMA, MeOH, 55 °C, 2−6 h. (*e*) NaBH$_4$, MeOH, rt, 1 h. R = tosylamide (**2−6**); 5-chlorothiophene-2-sulfonylamide (**7**). R$_1$ = *p*-chloro aniline (**2**); benzyl amine (**6** and **7**).

appropriately functionalized piperidone (**13** and **14**) and reacted under Strecker conditions with the aromatic or aliphatic amine in the presence of trimethylsilyl cyanide (TMSCN) to obtain aminonitrile derivatives (**15−17**). The nitrile group was then hydrolyzed under controlled conditions using concentrated sulfuric acid to achieve an amide function (**18−20**). A spirocyclization with dimethylformamide/dimethyl acetal (DMF−DMA) was then carried out (**21−23**). Finally, the C−N double bond was reduced with NaBH$_4$ in order to isolate the final products.

In the case of derivatives **3−5**, we used a commercially available spiropiperidinic compound, which was functionalized with aniline in the N_1 position. The final products were then obtained by acylating (**3** and **4**) or alkylating (**5**) the nitrogen in position N_8, as described in detail in Scheme 2, isolating the corresponding final compounds. The alkylating agent has been

Scheme 2. Synthesis of Compounds 3−5[a]
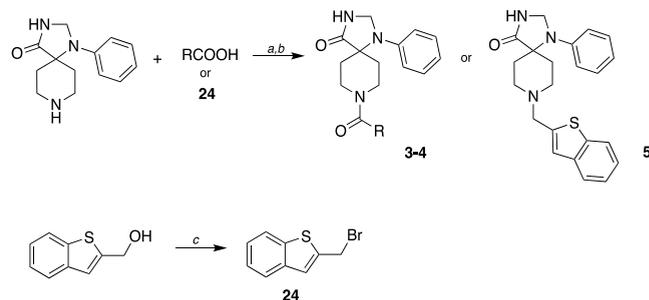
[a]Reaction conditions. (*a*) Oxalyl chloride, TEA, DMF gtt., THF, or DCM, 0 °C to rt, 18 h (**3** and **4**). (*b*) K$_2$CO$_3$, DMF, rt, 4 h (**5**). (*c*) PPh$_3$, CBr$_4$, DCM, 0 °C to rt, 3 h (**24**). R = 6-fluoropicolinoyl-amide (**3**); 1*H*-indole-2-carbonylamide (**4**).

prepared with a classical Appel reaction, permitting conversion from a primary alcohol to a bromide derivative (**24**).

Compound **8** (Scheme 3) has its own synthetic pathway. Piperidone was initially functionalized at position N_8 using benzoyl chloride to obtain compound **25**. Then, due to a treatment with TMSCN in methanol, a mixture of cyanohydrin (**26**) and its corresponding silyl ether derivative (**26a**) was obtained. The ether was then in situ hydrolyzed in acidic conditions to isolate intermediate **26**, which reacts with InBr$_3$ and benzyl amine, resulting in the amino-nitrile derivative **27**. The subsequent reaction steps, useful to obtain the final product **8**, implicate the same conditions as described above in Scheme 1.

Finally, derivatives **9−11** were obtained by using the appropriate sulfonyl chloride or benzoyl chloride to function-alize the nitrogen in the N_8 position. To derivatize the ketone by the Strecker reaction, a mixture of ammonium hydroxide and ammonium chloride was used to obtain a free primary amine at position N_1 (**30−32**). The synthetic pathway then proceeded with the hydrolysis of the nitrile group (**33−35**), cyclization with DMF/DMA (**36−38**), and subsequent reduction of the C−N double bond, as described in Scheme 4. At this point, protected *m*-hydroxy benzyl bromide (**46**) was reacted with the spiropiperidinic scaffold to obtain the suitably functionalized core at position N_8 (**39−41**). After reduction of the C−N double bond (**42** and **43**) and hydrolysis of the protecting group under acidic conditions, the compounds of interest **9−11** were isolated (Scheme 4).

**Biological Evaluation of Spiropiperidine Derivatives on HeLa Cells Using Cobalt−Calcein Assay.** To assess the efficacy of spiropiperidine derivatives in inhibiting Ca^{2+}-mediated mPTP opening, we measured their biological activity in HeLa cells by applying a calcein−cobalt assay protocol.[28] mPTP opening was stimulated by addition of the ionophore ionomycin, and the resulting kinetics were compared (see Figure 4).

As shown in Figure 4, addition of 1 μM ionomycin to cells pretreated with 1 μM compounds **2**, **6**, **7**, **9**, **10**, and **11** resulted in a significant desensitization of mPTP opening with the maximum effect achieved by compound **2** with an approximately 57% decrease. Furthermore, compounds **6** and **7** had important biological effects against channel opening. Compounds **3**, **4**, and **8** had the lowest or null effect: these data are consistent with those obtained using measurement of the membrane potential alteration with RPTEC cells, as specified in detail below.

Biological Evaluation of Spiropiperidine Derivatives on Renal Proximal Tubular Epithelial Cells. The general

Scheme 3. Synthesis of Compound 8[a]
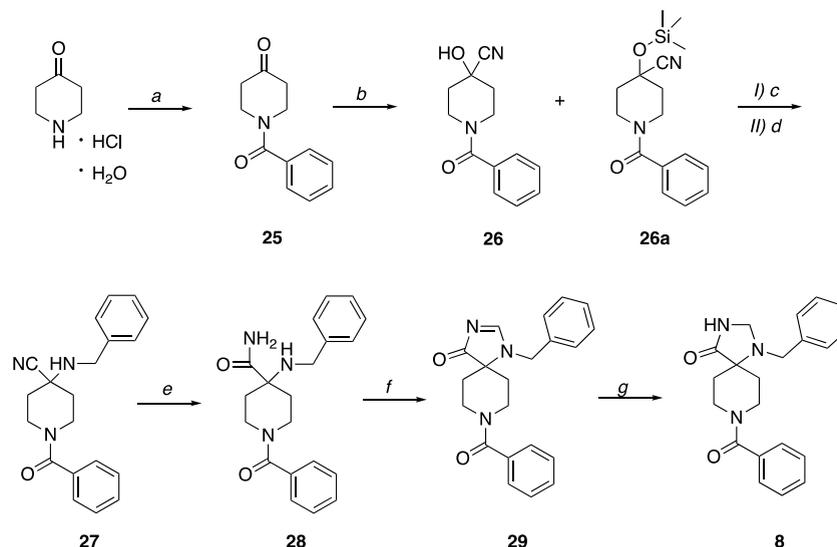
[a]Reaction conditions. (a) benzoyl-Cl, TEA, DCM, from 0 °C to rt, 18 h. (b) TMSCN, MeOH, rt, 18 h. (c) HCl $_{conc.}$, MeOH, 0 °C, 5 h (only for **26a**). (d) benzyl-NH$_2$, InBr$_3$, DCM, rt, 3 h. (e) H$_2$SO$_4$ conc., rt, 18 h. (f) DMF/DMA, MeOH, 55 °C, 2−6 h. (g) NaBH$_4$, MeOH, rt, 1 h.

Scheme 4. Synthesis of Compounds 9−11[a]
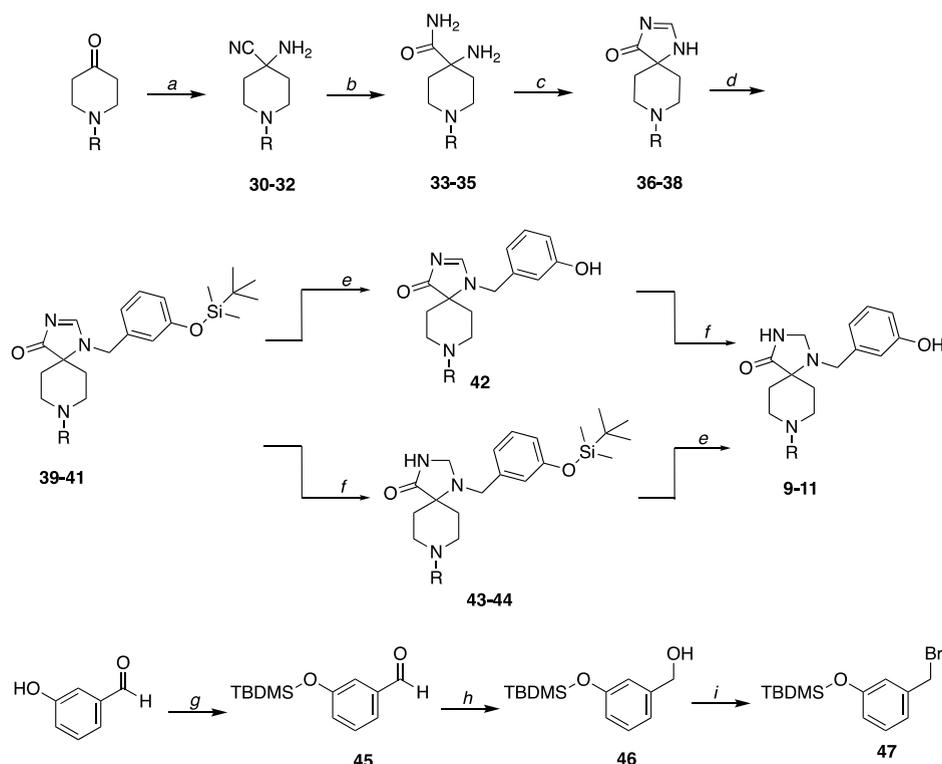
[a]Reaction conditions. (a) TMSCN, NH$_4^+$OH$^-$, NH$_4^+$Cl$^-$, $i$pr-OH, rt, 18 h. (b) H$_2$SO$_4$ conc., rt, 18 h. (c) DMF/DMA, MeOH, 55 °C, 2 h. (d) **47**, K$_2$CO$_3$, ACN, rt, 8 h. (e) HCl conc., MeOH, 0 °C, 5 h. (f) NaBH4, MeOH, from 0 °C to rt, 3 h. (g) TBDMSCl, imidazole, DCM, rt, 18 h. (h) NaBH$_4$, MeOH, 0 °C to rt, 3 h. (i) PPh$_3$, CBr$_4$, DCM, from 0 °C to rt, 3 h. R= tosylamide (**9**); 5-chlorothiophene-2-sulfonylamide (**10**); p-fluoro benzoyl amide (**11**).

aim of this study was to investigate the possibility of inhibiting mPTP opening. Stimulated by the good data described above, we tried to evaluate the activity of the molecules by analyzing another aspect resulting from the opening of the mPTP, namely, alteration of the cell membrane potential. Since available literature indicates that mPTP opening leads to the loss of the proton gradient,[29,30] a different test was used both on HeLa cells and on a more specific cell model, namely, the human renal proximal tubular epithelial cells (RPTECs). In this case, membrane depolarization or hyperpolarization has been monitored using Incucyte MMP (mitochondrial membrane potential) Orange Reagent (MMPOR see Figure 5). This
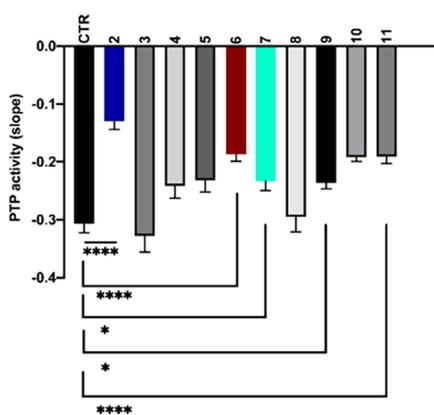
Figure 4. Statistics of PTP activity measurements by applying calcein—cobalt assay in HeLa cells pretreated with either DMSO (vehicle) or 1 μM compounds. Graph shows mean $\pm$ SEM. **** $p < 0.0001$, * $p < 0.05$.

compound is a cell-permeable, red-orange fluorescent dye that freely passes through cellular and mitochondrial membranes. Due to the large electrochemical H^+ gradient across the mitochondrial inner membrane, MMPOR accumulates in the mitochondrial matrix according to $\Delta\psi m$. Opening of mPTP, due to the introduction of an uncoupling agent such as FCCP, causes an efflux of dye from the mitochondria that manifests as a reduction of fluorescence intensity, which is easily measurable by fluorescence microscopy.

The protocol was set up with HeLa cells and then translated to primary cell cultures, RPTECs, as explained in the Materials and Methods. In Figure 5E, a representative experiment in the RPTECs cells pretreated with Incucyte MMPOR is shown. A clear fluorescence reduction follows the addition of FCCP as expected.

Oligomycin A is classified as a mPTP opening inhibitor that targets the c subunit of F_1/F_O ATP synthase. Accordingly, this compound was used as a positive control in these experiments.

Briefly, RPTECs were plated to reach a concentration of 6000 cells/well; successively, a staining solution was added to the cells for 15 min at 37 °C in a 5% CO_2 atmosphere. Once stained, negative controls were treated with 20 μM FCCP, and images were acquired every 5 s for a total of 15 min. On the other hand, different treatments and positive controls were first incubated with drugs (1 μM) or oligomycin A (1 μM) for other 15 min before acquiring images. Inhibition analysis was performed using a Carl Zeiss microscope with a 40×/0.6-N.A. Acquired data were analyzed using ImageJ and Python libraries. All statistical analyses were performed using one-way ANOVA with multiple comparisons performed by GraphPad Prism (p values are reported in the figure legends).

Every frame was analyzed by sketching the region of interest (ROI) over the stacked frames and calculating the pixel intensity of these regions. The resulting plots shown in Figure 5A−C present a curve for each ROI, on which was calculated the slope via linear interpolation between $t_0 = 15$ s and $t_1 = 180$ s. Finally, the mPTP inhibition (%) was calculated as follows

$$\text{mPTP inhibition (\%)} = 100 - \left(\frac{\text{slope\_drug}}{\text{slope\_control}} \times 100 \right)$$

As can be seen in Figure 5A, addition of FCCP in controls induces a clear mitochondrial depolarization, resulting in a loss of fluorescence within the first few seconds of the analysis.

Oligomycin A, as shown in Figure 5B, results in a mild protective effect, which is manifested in the persistence of fluorescence at 533 nm for a longer time period (still measurable in the same scale of tens to hundreds of seconds). Lastly, as shown in Figure 5C, pretreatment of the RPTECs with drug compound **6** not only modulates mitochondrial permeability positively, disfavoring mPTP formation, but also hyperpolarizes mitochondria. Indeed, hyperpolarization effects result in a consistent increase in fluorescence at the same wavelength. Finally, we can state that some compounds have yielded positive results on mPTP inhibition showing a larger effect with respect to the positive control oligomycin A. Among them we can highlight the most promising ones: **2**, **6**, and **7**, see Figure 5D.

It is to be noted that due to the hyperpolarization occurring upon treatment for some ligands (i.e., compounds **2** and **7**), the mPTP inhibition (%) measured with the formula described above exceeds the 100% threshold; thus, the activity of those compounds has been capped to 100%.

Optimized In Silico Binding Study of Spiropiperidine Compounds. According to the in vitro promising results obtained, deeper characterization of the binding mode between spiropiperidine compounds and ATP synthase F_O subunit was carried out using compound **6** as a probe (being one of the most active molecules). For this refinement, the novel Cryo-EM structure of the Human ATP synthase (PDB ID: 8H9J)[31] containing all of the subunits of the transmembrane F_O portion was used.

In fact, in the initial selection process, we presented the binding mode of compound **1** with a humanized C ring using the binding site of oligomycin A as a reference. However, that binding pose was found to be unstable over long molecular dynamics (MD) simulations. Hence, alternative binding sites have been investigated to find a more suitable complex in light of the different pharmacological properties of spiroderivatives with respect to oligomycin A,[32] suggesting that they have the same topological binding site but are not completely superimposable.

In Figure 6, the transmembrane F_O moiety is shown. In this complex, three chains of the c subunit interact with subunit a to give rise to two distinct and possible binding sites, here named 18a and 87a (according to the chains forming them).

On these sites, compound **6** has been docked via induced-fit docking, selecting residues L123, F115, and L117 of chains 1/8 and 8/7 according to the binding site to describe the boxes where the compound will be docked. IFD allows one to find a binding pose in the same topological position of the binding mode previously provided (Figure S2). Both complexes have been tested by performing 500 ns long MD simulation in 3 replicas.

Investigating the binding of compound **6** to binding site 18a, we observed that the complex formed is highly unstable. Remarkably, within just a few nanoseconds of the simulation, the ligand undergoes detachment from the binding site. This phenomenon can be attributed to a fundamental issue: the binding site's limited spatial capacity.

The structural intricacies of compound **6** are such that its benzyl group in position 1 becomes a pivotal player in the instability observed. As the ligand occupies binding site 18a, this particular group tends to intrude between the alpha helices of subunit a, as illustrated in Figure S1. This intrusion, however, comes at a cost: it distorts the native conformation of these alpha helices.

During the course of the MD simulations, it becomes evident that the alpha helices have a propensity to naturally revert to
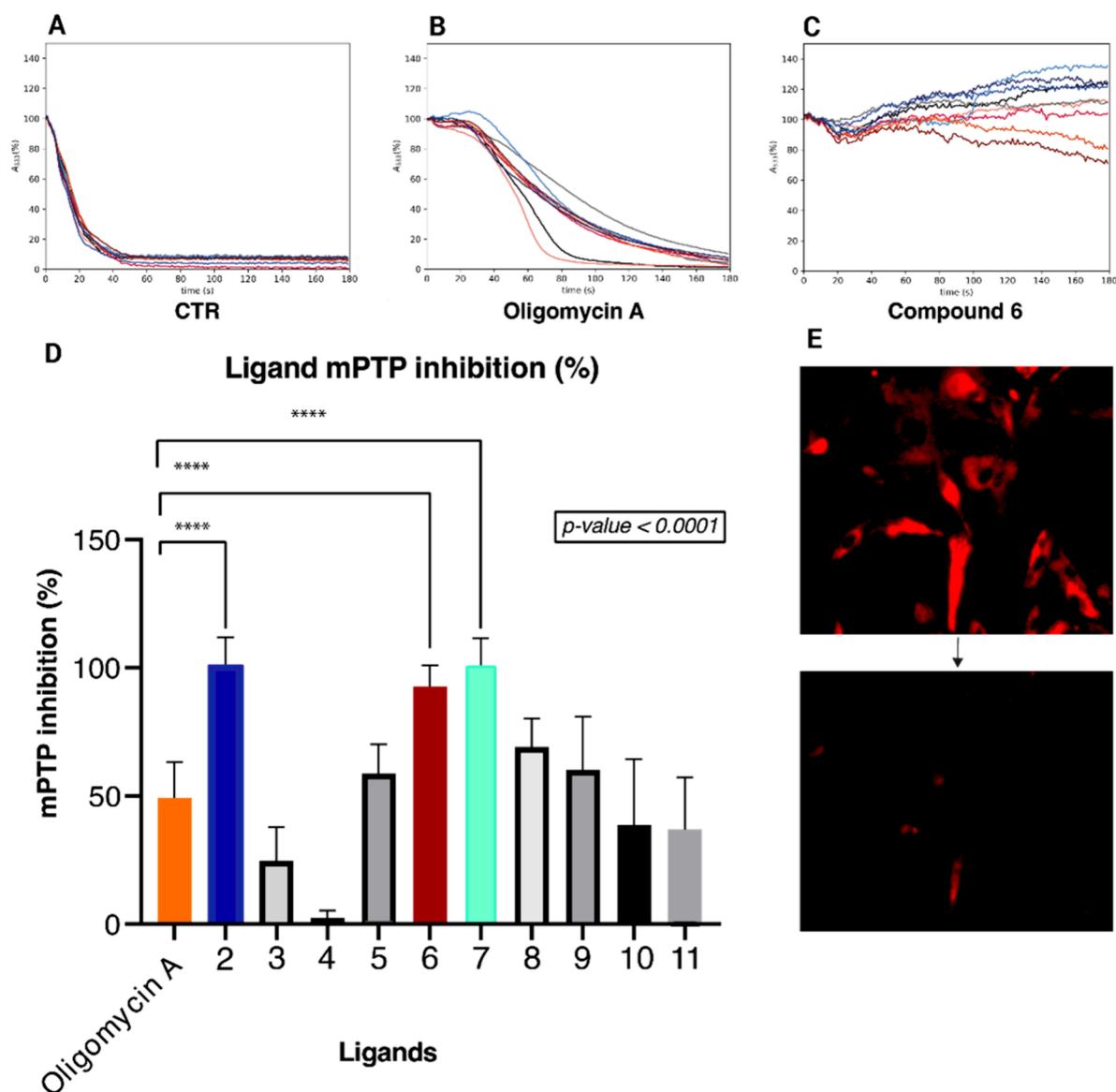
Figure 5. (A−C) Plots generated by image analysis on RPTECs: (A) control nontreated cells, (B) pretreated cells with oligomycin A, and (C) pretreated cells with compound **6**. (D) Ligand mPTP inhibition (%) plot of the tested compounds: (orange) oligomycin A; (blue, red, and cyan) most active candidates in mPTP opening inhibition on RPTECs (compounds **2**, **6**, and **7**, respectively). (E) RPTECs stained with Incucyte MMP Orange Reagent before (top) and after (bottom) the addition of FCCP. B shows a heavy depolarization induced by FCCP in control cells, meanwhile pretreated cells maintain their fluorescence (C and D), even hyperpolarizing (D).

their native, energetically favorable conformation. Unfortunately, this inherent tendency further exacerbates the unfavorable interactions with compound **6**, ultimately leading to its detachment from the binding site.

In essence, the limited spatial accommodation within binding site 18a combined with the structural clash induced by the compound **6** benzyl group culminates in the ligand's instability and detachment during the MD simulations.

Notably, a strikingly different outcome is observed when compound **6** is introduced to binding site 87a. In this scenario, the benzyl group encounters a more suitable and larger pocket, and as a result, no detachment occurs.

In Figure 7A and 7B, the most representative conformation obtained from the simulation is shown as well as the schematic binding (Figure 7C) and the interaction histograms obtained by analyzing the last 250 ns of three 500 ns MD simulations, Figure 7D.

Compared to the binding mode obtained from the IFD (Figure S1), the benzyl group (attached to N, position 1) makes space in a pocket inside subunit a, interacting hydrophobically with a:152Q and a:221Y. With this latter amino acid, a persistent π-stacking interaction is established between aromatic moieties. Then, a:152Q and a:221Y polar hydrogens form hydrogen bonds with the amine nitrogen and the sulfone moiety of the tosyl group. As regards the tosyl group, in position 8, it strongly interacts mostly with T-shape and sandwich π-stacking with 8:124F and 7:115F. The tosyl group, thanks to its sulfone group, can interact via a hydrogen bond with a:159R. Lastly, 8:117L and 8:113L make hydrophobic interactions with both the tosyl group and the core of the spiropiperidine scaffold. This binding mode allows this ligand to completely lose the interaction with the key residue of oligomycin interaction E119, making the binding independent from this residue.
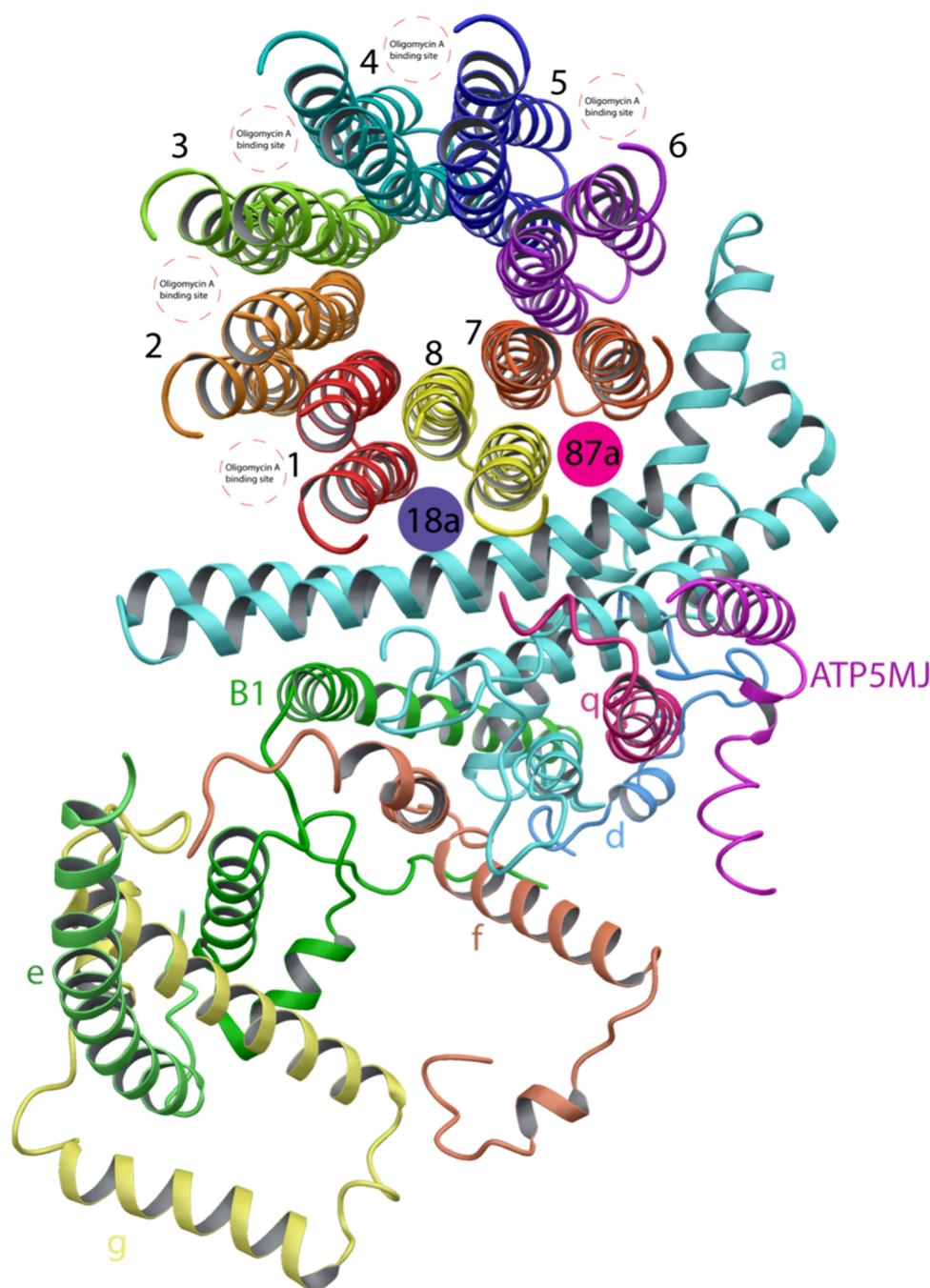
Figure 6. Transmembrane F$_O$ moiety of the ATP synthase, highlighting the oligomycin A binding sites (between c subunit chains) and the putative sites 18a and 87a formed together with subunit a chain. Chains are labeled as in the deposited structure (PDB ID: 8H9J).

This description is in accordance with the latest experimental results obtained by Pedriali et al.,[32] where the independence of the spiropiperidine compounds binding mode to the residue E119 was confirmed.

Pharmacophore Modeling. In order to generate the pharmacophore model, the most representative conformation of compound **6**, Figure 7B, was used. The binding pose was analyzed using the Phase[33] module in the Schrodinger suite.

As shown in Figure 8A, the key features for efficient binding to pocket 87a are as follows:

- The aromatic rings Ar1 and Ar2;

- The hydrophobic cores H1 and H2, respectively, the spiropiperidine scaffold and the methyl group of the tosyl moiety;
- The H-bond acceptor, A1 to interact with a:159R and a:221Y.

In Figure 8B−D, the sulfone-derived spiropiperidines are the ones that meet all conditions. Their geometry allows for simultaneous hydrogen-bond interactions and effective placement of the aromatic group within the hydrophobic pocket between chains 8 and 7. Moreover, both the phenyl and the benzyl groups (position 1) can fit into the hydrophobic pocket in subunit a, with the former (Figure 8B, compound 2, in pink) engaging in a T-shaped π-stacking interaction with a:221Y and
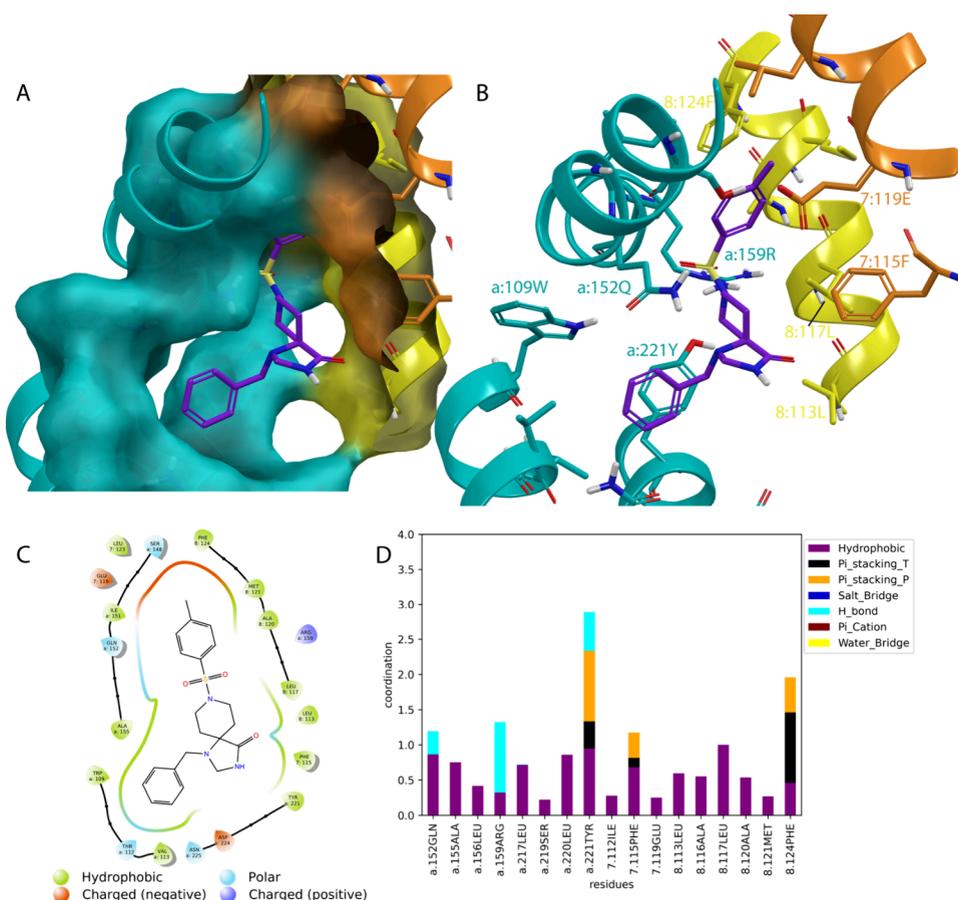
Figure 7. Compound **6** binding characterization. (A and B) Most representative conformation of compound **6** (in purple) in 87a shown as surface and zoomed-in views of the complex (PDB ID: 8H9J). (C) Binding scheme of the complex. (D) Interaction histograms of the compound **6**−87a pocket. Results include hydrophobic and polar contacts, hydrogen bonds, and salt bridges as determined by analyzing the last 250 ns of three 500 ns MD simulations.
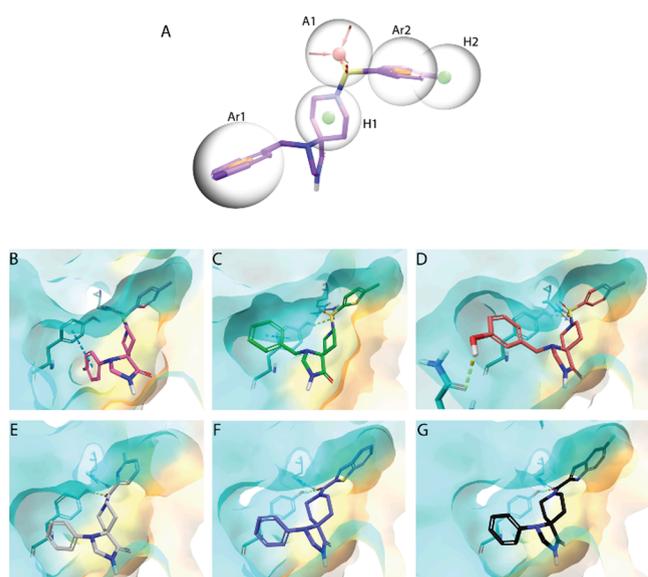

Figure 8. (A) Pharmacophore model as calculated onto the binding mode of compound **6**. (B, C, D, E, F, and G) Redocking of compounds **2**, **7**, **8**, **3**, **5**, and **4**, respectively, into the 87a binding site (PDB ID: 8H9J).

the latter (Figure 8C, compound **7**, in green) employing a sandwich π-stacking arrangement.

Turning our attention to compound **9** (Figure 8D, ligand in orange), which is the least active among the sulfone-derived compounds, it still meets all of the pharmacophore features except for Ar1. The presence of a hydroxyl group in the meta position to the benzyl group causes the moiety to shift away from a:221Y, favoring hydrogen-bond interactions with a:225N instead.

In contrast, carbonyl-derived spiropiperidine compounds exhibit lower activity compared to their sulfonic counterparts. This discrepancy can be attributed to the fact that the carbonyl group cannot engage simultaneously in hydrophobic and hydrogen-bond interactions. When the carbonyl oxygen forms a hydrogen bond with a:159R or a:221Y, the aromatic ring moves farther away from the hydrophobic pocket between chains 8 and 7, as demonstrated in Figure 8E for compound **3** (ligand in gray). Additionally, the carbonyl oxygen prefers interacting with the tyrosine hydroxyl rather than the a:159R guanidine, reducing the interaction of the aromatic moiety in position 8 with the pocket between chains 7 and 8.

Introducing the benzothiophene group in compound **5** (Figure 8F, ligand in light blue) enhances interaction with the c subunit because of its hindrance, leading to a correlated increase in activity.

However, bulkier groups do not yield improved biological activity. In fact, compound **4** (Figure 8G, ligand in black) was found to be inactive on RPTECs. The 5-fluoro indole carbonyl group, fitting into the c-ring groove, pushes the ligand

downward, improving interaction between the carbonyl and a:221Y hydroxyl, but it results in the loss of π-stacking interaction between tyrosine and the phenyl moiety in position 1. This rearrangement may be the underlying reason for its loss of inhibitory activity.

CONCLUSIONS

Ischemia—reperfusion injury (IRI) is a pathological condition that occurs after the restoration of blood flow in an ischemia event. The IRI is related to the opening of a mitochondrial transition pore (mPTP) that disrupt the cell homeostasis with the consequent cell death by apoptosis. Nowadays, all of the molecules tested for cardioprotective or nephroprotective purposes have failed in clinical trials. According to an in silico drug design starting from the X-ray crystal structure of the C ring cocrystallized with oligomycin A, we were able to generate a library of millions compounds.

Applying a high-throughput virtual screening protocol and standard precision and extra precision (XP) docking procedures combined with molecular dynamics, we selected 10 final compounds to be synthesized, considering different chemical strategies to explore the chemical space around the spiropiperidine core. Finally, in order to evaluate the biological properties of the selected compounds, two different biological testings have been set up, both in immortalized HeLa cell line and in the more specific renal proximal tubular epithelial cells (RPTECs). Among the spiropiperidine-selected molecules, compounds **2**, **6**, and **7** bearing the N^8 sulfonyl amide moiety showed the best inhibition activity on the mPTP opening. These experimental results were further analyzed computationally considering the interaction of these selected molecules with Human ATP synthase (PDB ID: 8H9J)[31] containing all of the subunits of the transmembrane F_O portion. This final refinement allowed us to identify the pharmacophore structure necessary to maximize the interaction with the human protein target. These encouraging results set the stage for their evaluation in an animal model of ischemic—reperfusion injury as a starting point for a proof of evidence-driven design of specific drugs for the treatment of IRI.

MATERIALS AND METHODS

Drug Design and Screening. The humanized C-ring model system was prepared via homology modeling using Prime, and all proteins were refined with the Protein Preparation Wizard[34] of the Schrodinger Suite. In order to find the binding pose of compound **1** (with humanized C ring) and compound **6** (with the human F_O subunit), induced-fit docking[35,36] was performed. As regards ligand library creation, building blocks have been retrieved from the ZINC15 database,[24] selecting compounds with a molecular weight of less than 250.

This set of molecules was filtered according to their functional groups; for the R_1 group, anilines and benzylamines were selected as they are reactants of the Strecker reaction (6755 molecules), while for the R_2 group, alkyl, sulfonyl, and acyl halides with an aromatic moiety (phenyl, benzofuranyl, indolyl, imidazolyl, etc.) were selected (690 reactants) to satisfy the structural constraint of forming π-stacking with the two phenylalanine residues F130,B and F124,A.

The library was made by combining these building blocks to the spiropiperidine scaffold via the Schrodinger Enumeration Library protocol as represented in Figure 9. The pool of compounds obtained was refined calculating molecular descriptors with QikProp and removing those molecules that did not satisfy Lipinski's rule of five. Finally, the pool was filtered for PAINS.[25]

The refined data set was prepared with LigPrep[37] before docking. HTVS, SP, and XP docking have been performed with Glide,[26]
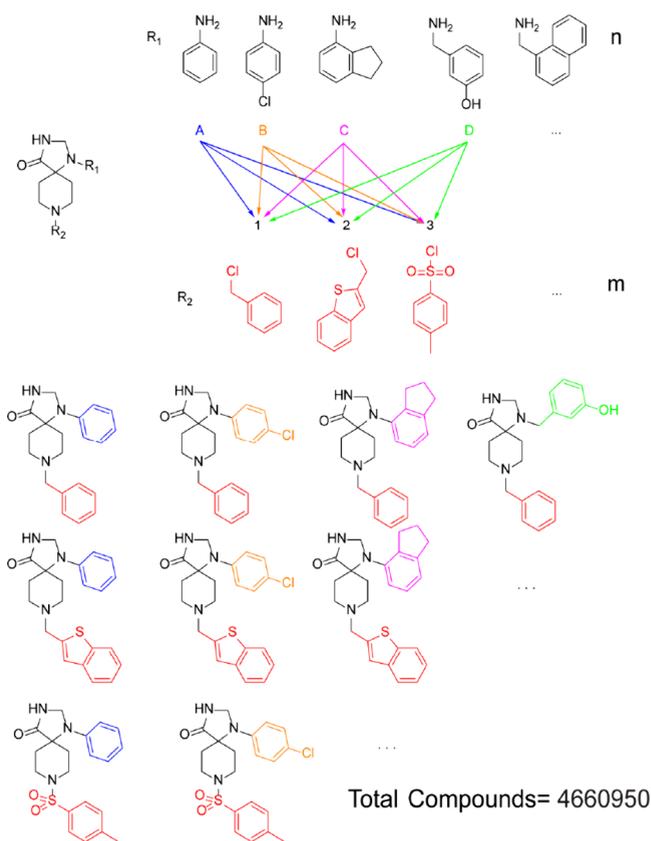

Figure 9. Representation of the strategy used to build the library. Every building block of one group (i.e., R_1: 6755 reactants) is added to the spiropiperidine scaffold and combined with all of the other building blocks of the other group (R_2: 690 reactants) giving more than 4.5 million compounds as result.

selecting the best 10% ligands of every docking procedure to be tested on the next one.

Molecular Dynamics Simulations. The coordinates of each protein—ligand complex were submitted to the CHARMM-GUI server[38] using the High Throughput Simulator tool[39] for membrane proteins. The topologies were generated using the CHARMM36m force field,[40] with the WYF parameter for cation—π interactions,[41] at the atomistic level using TIP3P as water solvent and the phospholipid bilayer of POPC (1-palmitoyl-2-oleoyl-sn-glycero-3-phosphocholine). The total charge of the system was neutralized by randomly substituting water molecules with K^+ ions and Cl^- ions to obtain neutrality with a 0.15 M salt concentration. For every system default minimization, equilibration and production CHARMM-GUI-supplied parameters have been used.

Analysis of Molecular Dynamics Trajectory. Molecular dynamics simulations have been analyzed using MDAnalysis[42] and PLIP[43] python libraries. Polar and hydrophobic interactions between the ligand and the protein residues were modeled as average coordination numbers via a continuous, differentiable switching function

$$\text{strength} = n_{\text{npc}} \sum_{ij} \frac{1 - (r_{ij}/r_0)^a}{1 - (r_{ij}/r_0)^b}$$

with the i and j indexes running over the interacting atoms within the peptide fragment of interest and those within a chosen protein residue with $0 \leq \text{strength} \leq n_i n_j$ (where n_i and n_j are the total number of atoms of the ligand fragment and the protein residue, respectively, able to make the chosen type of interaction). For hydrophobic interactions, only carbon atoms are considered; for polar interactions, only oxygens and nitrogens are considered. The same "strength" function was

calculated for salt bridges and π−cation and π−π interactions. In this case, $n_i = n_j = 1$ because virtual atoms are defined at the center of mass of the aromatic rings or charged groups; hence, $0 \leq$ strength ≤ 1. For hydrophobic, salt bridge, π−cation, and π−π interactions, $a = 6$, $b = 12$, and $r_0 = 6$, 5, 4, and 5.5 Å, respectively, while for polar interactions, $a = 8$, $b = 12$, and $r_0 = 2.5$. The chosen values of r_0 account for the typical interaction distance plus thermal motion's amplitude (e.g., ~4.5 Å + ~1.5 Å in the case of hydrophobic interactions). These coordination numbers (one per residue of the binding site) can be calculated on single structures as well as averaged along trajectories.

■ EXPERIMENTAL SECTION

Reaction progress and product mixtures were monitored by thin-layer chromatography (TLC) on silica gel (precoated F254 Macherey-Nagel plates) and visualized by a UV lamp (254 nm light source). The organic solutions from extractions were dried over anhydrous sodium sulfate. Chromatography was performed on Merck 230−400 mesh silica gel or using Isolera One (Biotage Sweden). ^{1}H, ^{13}C, DEPT, bidimensional (gCOSY), and heterocorrelated (gHMQC, gHMBC) NMR spectra were recorded on a VARIAN Mercury Plus 400 MHz spectrometer. Chemical shifts (δ) are reported in parts per million (ppm) using the peak of deuterated solvents as an internal standard, and coupling constants (J) are reported in Hertz. Splitting patterns are designed as follows: s, singlet; d, doublet; t, triplet; q, quartet; m, multiplet; b, broad. Melting points for purified products were determined in a glass capillary on a Stuart Scientific electrothermal apparatus SMP3 and are uncorrected. Mass spectra were recorded by an ESI single-quadrupole mass spectrometer Waters ZQ 2000 (Waters Instruments UK). For analytical controls, a Beckmann System Gold 168 HPLC apparatus was used with an LC column Kinetex 5-μm EVO C18 100 Å (250 Å, ~4.6 mm) and a variable-wavelength UV detector fixed to 220 nm. The analysis was conducted using two solutions, A and B, containing 100:0.1 H_2O:TFA and 40:60:0.1 H_2O:CH_3CN:TFA, respectively, with a gradient elution of 0−50% solution B over 30 min. The purity of all compounds was determined by HPLC and was greater than 95%. Mass spectrometric detection was carried out using an electrospray interface (ESI) operated in positive ionization mode. Nitrogen was used as a desolvation gas at a 300 L/h flow rate with the desolvation temperature set at 150 °C and the source temperature set at 130 °C.

General Procedure for the Synthesis of Compounds 2, 6, and 7. *1-Tosylpiperidin-4-one (13).* Commercially available 4-piperidone monohydrate hydrochloride (1 equiv) was suspended in a solution of H_2O and dioxane (1:2, 20 mL), and then Na_2CO_3 (2 equiv) was added. After 15 min, p-toluene sulfonyl chloride (1.1 equiv) was slowly put in the mixture. The reaction was stirred at room temperature for 8−18 h and monitored by TLC (A1P1) and MS-ESI. When complete, the dioxane was evaporated, and the aqueous phase was extracted with AcOEt (3 × 30 mL). The resulting solid was ground with Et_2O and then filtered to isolate the desired compound **13**. MS (ESI): m/z [M + H]${}^{+}$ 254.30. ^{1}H NMR (400 MHz, chloroform-d) δ 7.70−7.65 (m, 2H), 7.36−7.32 (m, 2H), 3.38 (t, J = 6.2 Hz, 4H), 2.53 (t, J = 6.3 Hz, 4H), 2.44 (s, 3H). ^{13}C NMR (101 MHz, chloroform-d) δ 206.08, 144.60, 133.83, 130.39, 128.01, 46.35, 41.12, 22.00.

1-((5-Chlorothiophen-2-yl)sulfonyl)piperidin-4-one (14). In a round-bottomed flask, piperidin-4-one monohydrated hydrochloride (1 equiv, 6,51 mmol) was suspended in DCM, and then TEA (3 equiv, 19.53 mmol) was added dropwise. After 15 min, the reaction was cooled to 0 °C and a solution of 5-chlorothiophene-2-sulfonyl chloride previously dissolved in DCM was slowly added. The reaction was allowed to warm to room temperature and stirred for 18 h. Once the reaction was completed, as indicated by TLC, the mixture was treated: the solvent was evaporated under vacuum and resuspended in DCM. The organic layer was extracted three times with water, dried over Na_2SO_4, filtered, and concentrated in vacuum. The crude brown oil was purified by flash chromatography (3:7 AcOEt/petroleum ether), obtaining the compound **14** as a yellowish solid (1.3 g, yield = 95%). MS (ESI) [M + H]${}^{+}$: 278,98. ^{1}H NMR (400 MHz, chloroform-d) δ 7.37 (d, J = 4.0 Hz, 1H), 6.99 (d, J = 4.0 Hz, 1H), 3.47 (d, J = 6.2 Hz,

4H), 2.57 (d, J = 6.4 Hz, 4H). ^{13}C NMR (101 MHz, chloroform-d) δ 205.10, 138.20, 134.79, 132.24, 127.37, 46.03, 40.55.

Intermediates 15−17. A solution of appropriate ketone (**13** or **14**) (1 equiv) in AcOH (5 mL) was cooled at 0 °C, and aniline or benzylamine was added dropwise (1 equiv). Then, 3 equiv of TMSCN was added. The mixture was stirred at room temperature until completion of the reaction. The progress of the reaction was monitored via TLC and MS-ESI. The mixture was then basified with NaOH 20% until pH = 10; after that, an extraction of the water phase was performed with DCM (3 × 30 mL). The reaction was then dried, and the organic solvent was evaporated: an amorphous solid was obtained, which was titrated with EtOH, to provide a yellowish/orange powder.

4-((4-Chlorophenyl)amino)-1-tosylpiperidine-4-carbonitrile. (15). MS (ESI): m/z [M + H]${}^{+}$ 390.49; 392.24. Yield: 66%. ^{1}H NMR (400 MHz, CDCl$_3$) δ 7.73−7.59 (m, 2H), 7.32 (ddt, J = 6.9, 1.3, 0.7 Hz, 2H), 7.25−7.12 (m, 2H), 6.76−6.66 (m, 2H), 6.01 (s, 1H), 3.37 (t, J = 7.1 Hz, 4H), 2.43 (s, 3H), 2.25 (t, J = 6.9 Hz, 3H).

4-(Benzylamino)-1-tosylpiperidine-4-carbonitrile (16). MS (ESI) [M + H]${}^{+}$: 369.15. Yield: 57%. ^{1}H NMR (400 MHz, CDCl$_3$) δ 7.68−7.61 (m, 2H), 7.37−7.33 (m, 2H), 7.32−7.24 (m, 5H), 3.86 (s, 2H), 3.59 (dt, J = 12.6, 4.6 Hz, 2H), 2.83 (ddd, J = 12.7, 10.1, 2.9 Hz, 2H), 2.46 (d, J = 0.8 Hz, 3H), 2.16−2.06 (m, 2H), 1.89 (ddd, J = 13.7, 10.1, 3.9 Hz, 2H). ^{13}C NMR (100 MHz, chloroform-d) δ 142.51, 139.53, 137.00, 129.62, 128.61, 128.43, 127.42, 127.26, 120.41, 53.49, 48.90, 43.23, 34.71, 21.53.

4-(Benzylamino)-1-((5-chlorothiophen-2-yl)sulfonyl)piperidine-4-carbonitrile (17). MS (ESI) [M + H^{+}]: 396.34. Yield: 84%. ^{1}H NMR (400 MHz, chloroform-d) δ 7.36−7.27 (m, 6H), 7.01 (d, J = 4.0 Hz, 1H), 3.89 (s, 2H), 3.62−3.53 (m, 2H), 2.98 (ddd, J = 12.5, 9.7, 3.1 Hz, 2H), 2.16 (dddd, J = 12.2, 6.0, 3.3, 1.6 Hz, 2H), 1.94 (ddd, J = 13.6, 9.7, 3.9 Hz, 2H). ^{13}C NMR (101 MHz, chloroform-d) δ 138.51, 136.58, 134.39, 132.11, 128.84, 128.46, 127.90, 127.39, 120.48, 54.97, 48.72, 42.33, 34.69.

Intermediates 18−20. Amino-nitrile intermediates (1 equiv) were solubilized in H_2SO_4 conc 96% at room temperature for 18 h. The proceeding of the reaction was monitored by TLC and MS-ESI. After completion of the reaction, the mixture was put at −10 °C and basified with $NH_4^{+}OH^{-}$ 28% until pH = 10−11. At this point, a white suspension was obtained. The ammonium salts were filtered through Celite with methanol, and the filtrate was concentrated to obtain an amorphous compound. Then, extraction with DCM (3 × 30 mL) and water was performed. The desired products **18−20** were isolated as white powders.

4-((4-Chlorophenyl)amino)-1-tosylpiperidine-4-carboxamide (18). MS (ESI): m/z [M + H]${}^{+}$ 408.31 ; 410.31. Yield: 94%

4-(Benzylamino)-1-tosylpiperidine-4-carboxamide (19). MS (ESI): m/z [M + H]${}^{+}$ 388.17. Yield: 94%. ^{1}H NMR (401 MHz, chloroform-d) δ 7.71−7.60 (m, 2H), 7.41−7.20 (m, 7H), 4.54−4.39 (m, 1H), 3.93 (dd, J = 8.6, 0.9 Hz, 2H), 3.35 (t, J = 7.1 Hz, 3H), 2.43 (t, J = 0.8 Hz, 4H), 2.17−1.90 (m, 4H). ^{13}C NMR (100 MHz, chloroform-d) δ 174.14, 142.79, 138.81, 136.80, 129.72, 128.61, 128.44, 127.42, 127.20, 60.79, 48.96, 43.16, 30.56, 21.53.

4-(Benzylamino)-1-((5-chlorothiophen-2-yl)sulfonyl)piperidine-4-carboxamide (20). MS (ESI) [M + H^{+}]: 414.32. Yield: 91%. ^{1}H NMR (400 MHz, chloroform-d) δ 7.38−7.21 (m, 6H), 6.98 (d, J = 4.0 Hz, 1H), 6.89 (s, 1H), 5.48 (s, 1H), 3.64 (s, 2H), 3.37−3.26 (m, 2H), 3.20 (ddd, J = 11.7, 7.7, 3.8 Hz, 2H), 2.26 (ddd, J = 12.3, 7.7, 3.9 Hz, 2H), 1.81 (ddd, J = 12.7, 7.5, 3.9 Hz, 2H). ^{13}C NMR (101 MHz, chloroform-d) δ 177.40, 139.37, 137.56, 134.78, 131.86, 128.83, 128.01, 127.66, 127.26, 58.88, 47.24, 42.88, 33.15.

Intermediates 21−23. To a solution of intermediates **18−20** (1 equiv) in methanol (10 mL), DMF/DMA (3 equiv) was added dropwise. The mixture was reacted at 55 °C for 6/10 h and monitored by MS-ESI. At the completion of the reaction, the solvent was evaporated, and a yellow solid was obtained. The desired products **21−23**, checked by TLC and MS-ESI, were used as such for the next step.

1-(4-Chlorophenyl)-8-tosyl-1,3,8-triazaspiro[4.5]dec-2-en-4-one (21). MS (ESI): m/z [M + H]${}^{+}$ 418.56; 420.31. Yield: 87%. ^{1}H NMR (400 MHz, chloroform-d) δ 8.23 (s, 1H), 7.65−7.60 (m, 2H), 7.51−7.45 (m, 2H), 7.35−7.29 (m, 2H), 7.13−7.07 (m, 2H), 3.70 (ddt, J =

12.2, 4.6, 1.9 Hz, 2H), 3.34 (dd, J = 12.3, 2.7 Hz, 2H), 2.44 (s, 3H), 2.10–2.00 (m, 2H), 1.84–1.77 (m, 2H).

1-Benzyl-8-tosyl-1,3,8-triazaspiro[4.5]dec-2-en-4-one (22). MS (ESI): m/z [M + H]$^+$ 398.15. Yield: 87%. ^{1}H NMR (400 MHz, chloroform-d) δ 7.75 (s, 1H), 7.68 (d, J = 7.5 Hz, 2H), 7.38–7.20 (m, 7H), 4.60 (d, J = 0.9 Hz, 2H), 3.39 (td, J = 7.2, 0.8 Hz, 4H), 2.43 (d, J = 1.0 Hz, 3H), 2.27–1.91 (m, 4H). ^{13}C NMR (100 MHz, chloroform-d) δ 181.17, 159.58, 142.79, 136.90, 129.53, 128.78, 127.66, 127.44, 127.23, 58.55, 49.78, 42.19, 28.70, 21.52.

1-Benzyl-8-((5-chlorothiophen-2-yl)sulfonyl)-1,3,8-triazaspiro-[4.5]dec-2-en-4-one (23). MS (ESI) [M + H$^+$]: 424.32. Yield: 86%. ^{1}H NMR (400 MHz, chloroform-d) δ 8.10 (s, 1H), 7.46–7.39 (m, 3H), 7.32 (d, J = 4.1 Hz, 1H), 7.26–7.22 (m, 2H), 6.98 (dd, J = 4.0, 0.4 Hz, 1H), 4.49 (s, 2H), 3.70 (ddd, J = 11.8, 4.5, 2.3 Hz, 2H), 3.43 (td, J = 12.3, 2.6 Hz, 2H), 2.08 (td, J = 13.0, 5.0 Hz, 2H), 1.69–1.63 (m, 2H). ^{13}C NMR (101 MHz, chloroform-d) δ 170.09, 137.92, 134.92, 133.71, 131.85, 129.68, 129.33, 128.15, 127.40, 76.98, 48.17, 40.35, 29.77.

Synthesis of Compounds 2, 6, and 7. General Procedures. The intermediates **21–23** (1 equiv) were suspended in methanol (10 mL), and the mixture was cooled at 0 °C with an ice bath. Then, NaBH$_4$ (1.2 equiv) was added slowly, and bubbling was observed. The reaction was monitored with MS-ESI upon completion. Then, the reaction was quenched with deionized water, the methanol was evaporated, and the resulting aqueous phase was extracted three times with DCM (3 × 30 mL). The combined organic phases were dried, and the solvent was evaporated. The resulting amorphous solid was titrated with Et$_2$O to obtain the desired products as white or yellow solids.

1-(4-Chlorophenyl)-8-tosyl-1,3,8-triazaspiro[4.5]decan-4-one (2). HRMS (ESI): calcd [M + H]$^+$ 420.11432; found 420.11328. Yield: 57%. Mp: 260–262 °C. HPLC t_R: 26.45 min. ^{1}H NMR (400 MHz, DMSO-d_6) δ 8.78 (s, 1H), 7.66 (d, J = 8.3 Hz, 2H), 7.53–7.43 (m, 2H), 7.25 (d, J = 9.1 Hz, 1H), 6.71 (d, J = 9.1 Hz, 2H), 4.54 (s, 2H), 3.64 (dd, J = 11.7, 5.0 Hz, 2H), 3.02 (d, J = 3.2 Hz, 1H), 2.47–2.39 (m, 5H), 1.67 (d, J = 13.7 Hz, 2H). ^{13}C NMR (101 MHz, DMSO-d_6) δ 174.73, 143.27, 141.67, 133.09, 129.72, 128.65, 127.22, 121.63, 115.36, 58.59, 57.45, 42.45, 27.80, 20.83.

1-Benzyl-8-tosyl-1,3,8-triazaspiro[4.5]decan-4-one (6). HRMS (ESI): calcd [M + H]$^+$ 400.16894; found 400.16914. Yield: 66%. Mp: 258–260 °C. HPLC t_R: 19.75 min. ^{1}H NMR (400 MHz, chloroform-d) δ 7.70–7.65 (m, 2H), 7.36–7.32 (m, 2H), 3.38 (t, J = 6.2 Hz, 4H), 2.53 (t, J = 6.3 Hz, 4H), 2.44 (s, 3H). ^{13}C NMR (101 MHz, chloroform-d) δ 206.08, 144.60, 133.83, 130.39, 128.01, 46.35, 41.12, 22.00.

1-Benzyl-8-((5-chlorothiophen-2-yl)sulfonyl)-1,3,8-triazaspiro-[4.5]decan-4-one (7). HRMS (ESI): calcd [M + H]$^+$ 426.07074; found 426.07048. Yield: 90%. Mp: 253–256 °C. HPLC t_R: 17.73 min. ^{1}H NMR (400 MHz, DMSO-d_6) δ 8.25 (s, 1H), 7.59 (d, J = 4.1 Hz, 1H), 7.40 (s, 1H), 7.33–7.26 (m, 5H), 3.79–3.77 (m, 2H), 3.67 (s, 2H), 3.54 (d, J = 11.4 Hz, 2H), 3.18–3.11 (m, 2H), 1.96–1.89 (m, 2H), 1.81 (d, J = 13.7 Hz, 2H). ^{13}C NMR (101 MHz, DMSO-d_6) δ 224.41, 209.72, 203.19, 133.31, 129.19, 128.80, 128.75, 127.54, 61.20, 50.22, 43.16, 28.49.

8-(6-Fluoropicolinoyl)-1-phenyl-1,3,8-triazaspiro[4.5]decan-4-one (3). To a solution of 6-fluoropicolinic acid (1 equiv, 2.16 mmol) in DCM at 0 °C, oxalyl chloride (1.2 equiv, 2.6 mmol) was added dropwise. A catalytic amount of DMF was added, and bubbling was observed. After 15 min, triethylamine (TEA, 1 equiv, 2.16 mmol) was added, followed by a solution of the commercially available 1-phenyl-1,3,8-triazaspiro[4.5]decan-4-one (1 equiv, 2.16 mmol), previously dissolved in DCM. The reaction was warmed to room temperature and stirred for 18 h. After the reaction was complete, as indicated by TLC and mass (ESI), the solvent was removed under vacuum and the residue was redissolved in DCM. The organic layer was washed three times with water, dried over Na$_2$SO$_4$, filtered, and concentrated in vacuum. The crude yellowish oil was purified by flash chromatography (9:1 AcOEt/petroleum ether), obtaining compound **3** as a white solid (235 mg, yield = 47%). HRMS (ESI): calcd [M + H]$^+$ 355.15648; found 355.15651. Mp: 248–250 °C. HPLC t_R: 19.75 min. ^{1}H NMR (400 MHz, chloroform-d) δ 7.91 (q, J = 7.8 Hz, 1H), 7.59 (ddd, J = 7.3, 2.2, 0.8 Hz, 1H), 7.34–7.27 (m, 2H), 7.04–6.99 (m, 1H), 6.93–6.86 (m, 2H), 6.80

(s, 1H), 4.78 (t, J = 4.2 Hz, 2H), 4.70–4.65 (m, 1H), 3.93–3.89 (m, 2H), 3.70–3.63 (m, 1H), 2.89–2.81 (m, 1H), 2.72–2.65 (m, 1H), 1.88 (d, J = 14.1 Hz, 1H), 1.76 (dd, J = 14.0, 3.5 Hz, 1H). ^{13}C NMR (101 MHz, chloroform-d) δ 177.44, 166.11, 163.28, 160.86, 152.71, 152.59, 142.73, 142.23, 129.67, 121.29, 119.86, 115.67, 111.13, 110.77, 59.70, 59.48, 43.89, 39.53, 29.84, 29.17. ^{19}F NMR (376 MHz, chloroform-d) δ −66.01, −66.60.

8-(5-Fluoro-1H-indole-2-carbonyl)-1-phenyl-1,3,8-triazaspiro-[4.5]decan-4-one (4). To a solution of 5-fluoro-1H-indole-2-carboxylic acid (1 equiv, 2.16 mmol) in THF at 0 °C, oxalyl chloride (1.2 equiv, 2.6 mmol) was added dropwise. A catalytic amount of DMF was added, and bubbling was observed. After 15 min, triethylamine (TEA, 1 equiv, 2.16 mmol) was added, followed by a solution of the commercially available 1-phenyl-1,3,8-triazaspiro[4.5]decan-4-one (1 equiv, 2.16 mmol), previously dissolved in THF. The reaction was warmed to room temperature and stirred for 18 h. After the reaction was complete, as indicated by TLC and mass (ESI), the solvent was removed under vacuum and the residue was redissolved in DCM. The organic layer was washed three times with water, dried over Na$_2$SO$_4$, filtered, and concentrated in vacuum. The crude yellowish oil was purified by flash chromatography (9.5:0.5 AcOEt/petroleum ether), obtaining compound **4** as a light brown solid (180 mg, yield = 36%). HRMS (ESI): calcd [M + H]$^+$ 393.17213; found 393.1719. Mp: 255–257 °C. HPLC t_R: 17.8 min. ^{1}H NMR (400 MHz, DMSO-d_6) δ 11.77 (d, J = 2.2 Hz, 1H), 8.85 (s, 1H), 7.39 (ddd, J = 25.2, 9.4, 3.6 Hz, 2H), 7.27–7.17 (m, 2H), 7.05 (td, J = 9.3, 2.6 Hz, 1H), 6.87–6.83 (m, 1H), 6.80–6.75 (m, 3H), 4.63 (s, 2H), 4.44–4.35 (m, 2H), 3.32 (s, 2H), 2.50–2.48 (m, 2H), 1.78 (d, J = 13.9 Hz, 2H). ^{13}C NMR (101 MHz DMSO-d_6) δ 175.76, 162.01, 158.26, 155.95, 143.12, 132.63, 131.81, 129.21, 127.01, 126.90, 118.08, 114.31, 113.26, 113.17, 111.96, 111.69, 105.62, 105.38, 103.64, 58.78, 58.57, 28.68. ^{19}F NMR (376 MHz DMSO-d_6) δ −123.88, −123.89.

8-(Benzo[b]thiophen-2-ylmethyl)-1-phenyl-1,3,8-triazaspiro-[4.5]decan-4-one (5). To a solution of 2-(bromomethyl)benzo[b]-thiophene **24** (1 equiv, 2.16 mmol) in DMF, K$_2$CO$_3$ (1.2 equiv, 2.6 mmol) was added followed by a solution of the commercially available 1-phenyl-1,3,8-triazaspiro[4.5]decan-4-one (1 equiv, 2.16 mmol), previously dissolved in DMF. The reaction was stirred for 4 h. After the reaction was complete, as indicated by TLC and mass (ESI), the solvent was removed under vacuum and the residue was redissolved in DCM. The organic layer was washed three times with water, dried over Na$_2$SO$_4$, filtered, and concentrated in vacuum. The crude yellowish oil was purified by flash chromatography (7:3 AcOEt/petroleum ether), obtaining compound **5** as a white and crystalline solid (1.1 g, yield = 84%). HRMS (ESI): calcd [M + H]$^+$ 378.16346; found 378.1632. Mp: 181–183 °C. HPLC t_R: 21.85 min. ^{1}H NMR (400 MHz, chloroform-d) δ 7.85–7.78 (m, 1H), 7.70 (dd, J = 7.4, 1.6 Hz, 1H), 7.37–7.25 (m, 5H), 7.17 (s, 1H), 7.01–6.94 (m, 3H), 6.92–6.87 (m, 1H), 4.75 (s, 2H), 3.88 (s, 2H), 2.92 (s, 2H), 2.76 (s, 1H), 1.76–1.69 (m, 3H). ^{13}C NMR (101 MHz, chloroform-d) δ 178.28, 144.91, 143.24, 140.16, 139.88, 129.74, 129.47, 124.18, 123.92, 123.20, 122.48, 121.83, 118.95, 115.23, 59.37, 59.27, 58.07, 49.94, 29.29.

2-(Bromomethyl)benzo[b]thiophene (24). To a solution of benzo-[b]thiophen-2-ylmethanol (1 equiv, 6.09 mmol) in dry DCM, triphenylphosphine (PPh$_3$, 1.2 equiv, 7.30 mmol) was added. Then, once PPh$_3$ was dissolved, the reaction was cooled to 0 °C and carbon tetrabromide (CBr$_4$, 1.2 equiv, 7.30 mmol) was added slowly and in a small portion. The reaction was warmed to room temperature and monitored via TLC. After 3 h, the solvent was evaporated under vacuum and the crude compound was purified by chromatographic column (1:9 AcOEt:petroleum ether). The purified compound was obtained as a white crystalline solid in 70% yield, and it was not appreciable via MS-ESI analysis. ^{1}H NMR (400 MHz, chloroform-d) δ 7.81–7.77 (m, 1H), 7.75–7.71 (m, 1H), 7.37–7.31 (m, 3H), 4.79 (d, J = 0.7 Hz, 2H). ^{13}C NMR (101 MHz, chloroform-d) δ 141.23, 140.75, 139.36, 125.17, 124.78, 124.64, 124.00, 122.61, 27.41.

1-Benzoylpiperidin-4-one (25). In a round-bottomed flask, piperidin-4-one monohydrated hydrochloride (1 equiv, 6,51 mmol) was suspended in DCM, and then TEA (3 equiv, 19,53 mmol) was added dropwise. After 1 h, the reaction was cooled to 0 °C and a

solution of benzoyl chloride (3 equiv, 19.53 mmol) previously dissolved in DCM was slowly added. The reaction was allowed to warm to room temperature and stirred for 18 h. Once the reaction was complete, as indicated by TLC, the mixture was treated: the solvent was evaporated under vacuum and resuspended in DCM. The organic layer was extracted three times with water, dried over Na_2SO_4, filtered, and concentrated in vacuum. The crude brown oil was purified by flash chromatography (3:7 AcOEt/petroleum ether), obtaining compound **24** as a white solid (1.3 g, yield = 57%). MS (ESI) $[M + H]^+$: 204.38. ^{1}H NMR (400 MHz, chloroform-*d*) δ 7.59–7.29 (m, 5H), 3.87 (d, *J* = 64.0 Hz, 4H), 2.50 (s, 4H). ^{13}C NMR (101 MHz, chloroform-*d*) δ 206.82, 171.08, 135.26, 130.39, 128.82, 127.09, 42.20, 41.64, 41.36, 40.86.

1-Benzoyl-4-hydroxypiperidine-4-carbonitrile (26). In an argon environment, ketone **25** (1 equiv, 816 mg, 4.02 mmol) was dissolved in distilled DCM. Next, InBr$_3$ (10.1 equiv, 42.53 mg, 0.40 mmol) was added, and it was completely dissolved for 5–10 min. Then, TMSCN (2 equiv, 1.01 mL, 8.04 mmol) was added dropwise. This was allowed to react at room temperature for 18 h, monitoring the reaction by TLC (A7P3) and mass spectrometry (ESI). Then, the distilled DCM was evaporated and extracted in DCM/H$_2$O deionized. After drying and evaporating the solvent, cyanohydrin **26** was isolated from its silyl derivative **26a** by column chromatography using a petroleum ether/AcOEt (3:7) eluent mixture. Finally, the silyl derivative was deprotected by acid hydrolysis: it was diluted in MeOH (10 mL), the flask was placed in an ice bath, and HCl solution was added dropwise until pH acid. The organic solvent was evaporated; this was extracted with deionized water and AcOEt and dried, and the organic solvent was evaporated. The cyanohydrin derivative **26** was obtained as a white solid in 78% yield. MS (ESI) $[M + H^+]$: 231.34. ^{1}H NMR (400 MHz, chloroform-*d*) δ 7.56–7.37 (m, 5H), 4.86 (s, 1H), 3.77–3.57 (m, 4H), 2.34 (t, *J* = 7.1 Hz, 4H). ^{13}C NMR (101 MHz, chloroform-*d*) δ 170.36, 136.22, 130.67, 128.93, 127.63, 120.42, 66.15, 41.22, 39.00.

1-Benzoyl-4-(benzylamino)piperidine-4-carbonitrile (27). Compound **26** was dissolved in DCM (10 mL), and InBr$_3$ (0.1 equiv) was added. Next, benzylamine (1.5 equiv) was added dropwise. This reaction was allowed to react at room temperature for 3 h, keeping the reaction monitored by TLC and mass spectrometry (ESI). Upon completion, the DCM was evaporated and extracted with DCM and NaHCO$_{3sat}$ (3 × 30 mL). After drying and evaporating the solvent, the product of interest was isolated by column chromatography using a petroleum ether/AcOEt (1:1) eluent mixture. Finally, the organic solvent was evaporated, resulting in the desired amino-nitrile derivative **27** as a white solid in 81% yield. MS (ESI) $[M + H^+]$: 320.38. ^{1}H NMR (400 MHz, chloroform-*d*) δ 7.47–7.26 (m, 10H), 4.37 (s, 1H), 3.93 (s, 2H), 3.77 (s, 1H), 3.48 (p, *J* = 5.8, 4.5 Hz, 2H), 2.19–2.09 (m, 1H), 2.00 (s, 1H), 1.88 (s, 1H). ^{13}C NMR (101 MHz, chloroform-*d*) δ 170.41, 138.60, 135.37, 129.98, 128.63, 128.38, 127.70, 126.89, 120.74, 55.90, 48.91, 43.72.

1-Benzoyl-4-(benzylamino)piperidine-4-carboxamide (28). Amino-nitrile intermediate **27** (1 equiv) was solubilized in H$_2$SO$_{4\ conc}$ 96% at room temperature for 18 h. The proceeding of the reaction was monitored by TLC and MS-ESI. After completion of the reaction, the mixture was put at −10 °C and basified with NH$_4^+$OH$^-$ 28% until pH = 10–11. At this point, a white suspension was obtained. The ammonium salts were filtered through Celite with methanol, and the filtrate was concentrated to obtain an amorphous mixture. Then, extraction with DCM (3 × 30 mL) and water was performed. The desired product **28** was isolated as a white powder in 80% yield. MS (ESI) $[M + H^+]$: 338.18. ^{1}H NMR (400 MHz, acetone-*d*$_6$) δ 7.82–6.86 (m, 9H), 6.45 (s, 1H), 3.98 (d, *J* = 59.3 Hz, 1H), 3.65 (s, 2H), 3.55 (d, *J* = 11.0 Hz, 2H), 1.78 (d, *J* = 38.7 Hz, 2H). ^{13}C NMR (101 MHz, acetone-*d*$_6$) δ 177.13, 169.25, 140.91, 137.04, 129.15, 128.25, 128.16, 126.87, 126.70, 59.97, 47.12, 43.52, 37.79, 33.02, 32.60.

8-Benzoyl-1-benzyl-1,3,8-triazaspiro[4.5]dec-2-en-4-one (29). To a solution of intermediate **28** (1 equiv) in methanol (10 mL), DMF/DMA (3 equiv) was added dropwise. The mixture was reacted at 55 °C for 6/10 h and monitored by MS-ESI. At the completion of the reaction, the solvent was evaporated, and a yellow solid was obtained in 93% yield. The cyclized desired product **29**, checked by TLC and MS-ESI, was used as such for the next step. MS (ESI) $[M + H^+]$: 348.27. ^{1}H

NMR (400 MHz, chloroform-*d*) δ 8.09 (s, 1H), 7.48–7.32 (m, 8H), 7.25 (dt, *J* = 7.3, 2.0 Hz, 2H), 4.66 (d, *J* = 13.1 Hz, 1H), 4.49 (d, *J* = 10.2 Hz, 2H), 4.03 (s, 1H), 3.75 (s, 1H), 3.66–3.58 (m, 1H), 2.02 (q, *J* = 14.5, 7.6 Hz, 2H), 1.72 (d, *J* = 16.9 Hz, 2H), 1.52 (s, 1H). ^{13}C NMR (101 MHz, chloroform-*d*) δ 191.97, 170.73, 169.05, 135.53, 133.43, 130.01, 129.60, 129.30, 128.67, 128.35, 127.00, 63.36, 48.41, 41.68, 36.06, 31.01, 29.77.

8-Benzoyl-1-benzyl-1,3,8-triazaspiro[4.5]decan-4-one (8). Intermediate **29** (1 equiv) was suspended in methanol (10 mL), and the mixture was cooled at 0 °C with an ice bath. Then, NaBH$_4$ (1.2 equiv) was added slowly, and bubbling was observed. The reaction was monitored with MS-ESI for completion. Then, the reaction was quenched with deionized water, the methanol was evaporated, and the resulting aqueous phase was extracted three times with DCM (3 × 30 mL). The combined organic phases were dried, and the solvent was evaporated. The resulting amorphous solid was titrated with Et$_2$O to obtain the desired product **8** as a yellowish solid in 88% yield. HRMS (ESI): calcd $[M + H]^+$ 350.1863; found 350.18646. Mp: 191−193 °C. HPLC *t*$_R$: 20.70 min. ^{1}H NMR (400 MHz, DMSO-*d*$_6$) δ 8.27 (s, 1H), 7.44 (dq, *J* = 2.6, 1.6 Hz, 5H), 7.33 (d, *J* = 4.4 Hz, 4H), 7.26 (ddd, *J* = 8.7, 5.1, 3.6 Hz, 1H), 4.38 (s, 1H), 3.81 (s, 2H), 3.77−3.61 (m, 3H), 1.81 (s, 3H), 1.66 (s, 1H). ^{13}C NMR (101 MHz, DMSO-*d*$_6$) δ 176.82, 169.07, 138.59, 136.41, 129.26, 128.34, 128.29, 127.02, 126.66, 60.79, 59.02, 49.94, 43.49, 37.92, 29.51, 28.43.

General Procedure for the Synthesis of Monospiranic Compounds 9−11. Functionalization of piperidone chlorhydrate monohydrate followed the procedures previously described to obtain intermediates **13**, **14**, and **24** using the appropriate sulfonyl chloride or benzoyl chloride to obtain the desired product.

Intermediates 30−32. In a round-bottomed flask, a solution of ammonium chloride (NH$_4$Cl, 1.3 equiv, 3.08 mmol) in ammonium hydroxide (NH$_4$OH, 10 equiv, 23.7 mmol) was added. Then, TMSCN (1.25 equiv, 2.96 mmol) was dropped in. Immediately after, a solution of appropriately functionalized piperidone (1 equiv, 2.37 mmol) previously dissolved in MeOH was added to the mixture. The reaction was stirred for 18 h and monitored via TLC and MS (ESI). Upon completion of the reaction, the solvent was evaporated, and the residue was diluted with water; the aqueous phase was extracted three times with AcOEt, dried over Na$_2$SO$_4$ anhydrous, filtered, and evaporated. The amino-nitrile derivative was obtained as a white solid without need for further purifications.

4-Amino-1-tosylpiperidine-4-carbonitrile (30). MS (ESI) $[M + H]^+$: 279.10. Yield: 90%. ^{1}H NMR (400 MHz, DMSO-*d*$_6$) δ 7.69−7.61 (m, 2H), 7.50−7.44 (m, 2H), 3.22 (ddd, *J* = 11.4, 5.5, 2.2 Hz, 2H), 2.75 (ddd, *J* = 11.9, 8.4, 3.3 Hz, 2H), 2.59 (s, 2H), 2.43 (s, 3H), 2.02−1.92 (m, 2H), 1.70 (ddd, *J* = 12.9, 8.5, 3.6 Hz, 2H). ^{13}C NMR (101 MHz, DMSO-*d*$_6$) δ 143.73, 132.21, 129.91, 127.49, 123.72, 48.05, 41.94, 35.22, 21.02.

4-Amino-1-((5-chlorothiophen-2-yl)sulfonyl)piperidine-4-carbonitrile (31). Yield: 91%. ^{1}H NMR (400 MHz, DMSO-*d*$_6$) δ 7.60 (d, *J* = 4.1 Hz, 1H), 7.40 (d, *J* = 4.1 Hz, 1H), 3.26 (ddd, *J* = 11.5, 7.3, 3.8 Hz, 2H), 2.94−2.85 (m, 2H), 2.64 (s, 2H), 2.03−1.97 (m, 2H), 1.75 (ddd, *J* = 12.9, 8.2, 3.6 Hz, 2H). ^{13}C NMR (101 MHz, DMSO-*d*$_6$) δ 135.68, 133.56, 133.11, 128.86, 123.69, 47.85, 41.97, 35.02.

4-Amino-1-(4-fluorobenzoyl)piperidine-4-carbonitrile (32). MS (ESI) $[M + H]^+$: 238.11. Yield: 71%. ^{1}H NMR (400 MHz, DMSO-*d*$_6$) δ 7.52−7.45 (m, 2H), 7.33−7.21 (m, 2H), 3.76 (d, *J* = 166.2 Hz, 2H), 3.25 (m, 2H), 2.69 (s, 2H), 1.95 (d, *J* = 14.3 Hz, 2H), 1.63 (s, 2H). ^{13}C NMR (101 MHz, DMSO-*d*$_6$) δ 168.13, 163.74, 161.29, 132.28, 129.47, 129.39, 124.01, 115.48, 115.26, 49.26, 36.14, 36.05. ^{19}F NMR (376 MHz, DMSO-*d*$_6$) δ −111.25.

Synthesis of Intermediates 33−35. Amino-nitrile derivatives **30−32** were dissolved in H$_2$SO$_4$ (96% w/w, 3 mL), and the mixture was stirred at room temperature for 18 h. After the reaction was complete, as indicated by MS (ESI), it was slowly basified (pH > 10) by dropwise addition of a NH$_4$OH solution (30% w/w) while maintaining the temperature between −10 and 0 °C, cooling the round-bottomed flask with a mixture of water and salt. Then, at pH > 10, the mixture was diluted with CH$_3$OH, and the ammonium salts were filtered away on a pad of Celite. Subsequently, the filtrate was evaporated under vacuum,

and the resulting yellowish oil was extracted five times with CH_2Cl_2 (20 mL). The organic layer was washed with water (2×10 mL) and brine (1×10 mL). After drying over Na_2SO_4, the solvent was evaporated under reduced pressure to yield a solid residue, which was triturated with Et_2O and filtered to isolate the carboxamide derivative as a pale-yellow solid. The final compound was used in the next step without further purification.

4-Amino-1-tosylpiperidine-4-carboxamide (33). MS (ESI) [M + H]$^+$: 297.11. Yield: 88%. ^{1}H NMR (400 MHz, DMSO-d_6) δ 7.69–7.53 (m, 2H), 7.48–7.41 (m, 2H), 7.35 (s, 1H), 6.94 (s, 1H), 3.27 (dt, J = 11.4, 4.1 Hz, 2H), 2.68 (td, J = 11.4, 2.9 Hz, 2H), 2.42 (s, 3H), 1.90 (ddd, J = 13.3, 11.3, 4.3 Hz, 2H), 1.69 (s, 2H), 1.41 (dd, J = 13.5, 3.6 Hz, 2H). ^{13}C NMR (101 MHz, DMSO-d_6) δ 179.24, 143.36, 132.66, 129.79, 127.47, 53.89, 41.82, 33.49, 21.01.

4-Amino-1-((5-chlorothiophen-2-yl)sulfonyl)piperidine-4-carboxamide (34). MS (ESI): [M + H]$^+$ = 323.02. Yield: 85%. ^{1}H NMR (400 MHz, DMSO-d_6) δ 7.55 (d, J = 4.1 Hz, 1H), 7.39 (t, J = 4.8 Hz, 2H), 6.99 (s, 1H), 3.32 (d, J = 7.5 Hz, 2H with D$_2$O), 2.84 (td, J = 11.5, 2.9 Hz, 2H), 1.94 (ddd, J = 13.4, 11.5, 4.4 Hz, 2H), 1.81 (s, 2H), 1.49–1.42 (m, 2H). ^{13}C NMR (101 MHz, DMSO-d_6) δ 179.11, 135.27, 134.09, 132.71, 128.68, 53.80, 41.88, 33.38.

4-Amino-1-(4-fluorobenzoyl)piperidine-4-carboxamide (35). MS (ESI): [M + H]$^+$: 265.12. Yield: 66%. ^{1}H NMR (400 MHz, DMSO-d_6) δ 7.51–7.37 (m, 3H), 7.32–7.23 (m, 2H), 6.98 (s, 1H), 4.12 (s, 1H), 1.95 (s, 2H), 1.84 (s, 2H), 1.35 (d, J = 45.8 Hz, 2H). ^{13}C NMR (101 MHz, DMSO-d_6) δ 179.27, 167.91, 163.62, 161.17, 132.73, 129.29, 129.21, 115.47, 115.25, 55.14, 43.36, 37.68, 34.72, 33.95. ^{19}F NMR (376 MHz, DMSO-d_6) δ −111.52.

Synthesis of Intermediates 36−38. Amino-amidic derivatives **33−35** (1 equiv, 2.16 mmol) were dissolved in MeOH; then, dimethylformamide dimethylacetal (DMF/DMA, 3 equiv, 3.24 mmol) was added dropwise. The mixture was stirred at 55 °C for 5 h. The volatile fraction was evaporated under reduced pressure to yield a solid residue, which was crystallized with acetone to yield a pale-yellow solid. The obtained raw product was checked by MS-ESI and TLC and was used as such in the next step.

8-Tosyl-1,3,8-triazaspiro[4.5]dec-2-en-4-one (36). MS (ESI): [M + H]$^+$ = 324.02. Yield: 85%. ^{1}H NMR (400 MHz, chloroform-d) δ 7.75 (s, 1H), 7.68–7.61 (m, 2H), 7.34–7.29 (m, 2H), 3.73 (dt, J = 11.4, 4.0 Hz, 2H), 2.87 (td, J = 11.6, 2.8 Hz, 2H), 2.43 (s, 3H), 2.11–2.01 (m, 2H), 1.53 (d, J = 13.6 Hz, 2H). ^{13}C NMR (101 MHz, chloroform-d) δ 185.31, 149.26, 143.77, 133.30, 129.89, 127.73, 67.03, 42.22, 32.12, 21.61.

8-((5-Chlorothiophen-2-yl)sulfonyl)-1,3,8-triazaspiro[4.5]dec-2-en-4-one (37). MS (ESI): [M + H]$^+$ = 333,10. Yield: 81%. ^{1}H NMR (400 MHz, DMSO-d_6) δ 7.96 (s, 1H), 7.60 (d, J = 4.0 Hz, 1H), 7.40 (d, J = 4.0 Hz, 1H), 3.56 (dd, J = 10.2, 5.9 Hz, 2H), 2.84 (dd, J = 11.5, 2.9 Hz, 2H), 1.77 (td, J = 12.5, 11.5, 4.2 Hz, 2H), 1.46 (d, J = 13.5 Hz, 2H).

8-(4-Fluorobenzoyl)-1,3,8-triazaspiro[4.5]dec-2-en-4-one (38). MS (ESI): [M + H]$^+$ = 275.11. ^{1}H NMR (400 MHz, DMSO-d_6) δ 8.02 (s, 1H), 7.54–7.44 (m, 2H), 7.30–7.20 (m, 2H), 3.33 (s, 4H), 1.68 (s, 2H), 1.37 (s, 2H).

Synthesis of Intermediates 39−41. To a solution of the appropriate compound **36−38**, 1 equiv, 2.14 mmol) in acetonitrile (DMF, 5 mL) at 0 °C, potassium carbonate (K_2CO_3, 1 equiv, 2.14 mmol) was added. Then, (3 (bromomethyl)phenoxy)(*tert*-butyl)-dimethylsilane (compound **46** described below, 0.9 equiv, 1.93 mmol) previously dissolved in DMF was also dropped in. The mixture was allowed to warm to room temperature and stirred for 7 h, monitoring the progress via TLC and MS (ESI). Upon completion of the reaction, the solvent was evaporated, and the crude compound was resuspended in water. The aqueous phase was extracted four times with DCM, dried over Na_2SO_4, filtered, and evaporated. The residue was purified by flash chromatography (9:1 AcOEt/petroleum ether), obtaining the final products **39−41** as transparent amorphous compounds.

1-(3-((tert-Butyldimethylsilyl)oxy)benzyl)-8-tosyl-1,3,8-triazaspiro[4.5]dec-2-en-4-one (39). MS (ESI): [M + H]$^+$ = 528.23. Yield: 50%. ^{1}H NMR (400 MHz, DMSO-d_6) δ 8.05 (s, 1H), 7.65 (d, J = 7.9 Hz, 2H), 7.47 (d, J = 7.9 Hz, 2H), 7.21 (t, J = 7.8 Hz, 1H), 6.82–6.74 (m, 2H), 6.68 (s, 1H), 4.55 (s, 2H), 3.54 (d, J = 11.4 Hz, 2H), 2.67

(t, J = 11.2 Hz, 2H), 2.42 (s, 3H), 1.83–1.70 (m, 2H), 1.41 (d, J = 13.3 Hz, 2H), 0.96–0.88 (m, 9H), 0.15 (s, 6H). ^{13}C NMR (101 MHz, DMSO-d_6) δ 183.16, 155.31, 153.81, 143.70, 138.32, 132.30, 129.98, 127.52, 120.20, 119.10, 118.60, 66.96, 43.33, 42.01, 31.57, 25.51, 21.02, 17.92, −4.58.

1-(3-((tert-Butyldimethylsilyl)oxy)benzyl)-8-((5-chlorothiophen-2-yl)sulfonyl)-1,3,8-triazaspiro[4.5]dec-2-en-4-one (40). MS (ESI): [M + H]$^+$ = 554.13. Overall yield: 73%. ^{1}H NMR (400 MHz, DMSO-d_6, deprotected and protected compound mixture) δ 8.10 (s, 1H), 8.07 (s, 0H), 7.64–7.58 (m, 1H), 7.40 (d, J = 4.1 Hz, 1H), 7.22 (t, J = 7.9 Hz, 1H), 7.13 (t, J = 7.8 Hz, 0H), 6.85–6.69 (m, 3H), 6.68–6.56 (m, 1H), 4.58 (s, 2H), 4.54 (s, 0H), 3.57 (t, J = 6.1 Hz, 3H), 2.95–2.80 (m, 3H), 1.82 (td, J = 12.6, 10.9, 4.3 Hz, 3H), 1.48 (d, J = 13.4 Hz, 3H), 0.92 (s, 10H), 0.84 (s, 2H), 0.15 (s, 6H), −0.04 (s, 1H). ^{13}C NMR (101 MHz, DMSO-d_6, deprotected and protected compound mixture) δ 183.09, 155.33, 154.01, 138.31, 135.67, 133.70, 133.09, 129.99, 128.85, 120.22, 119.12, 118.64, 66.80, 43.39, 42.12, 31.43, 25.81, 25.52, 18.73, 17.92, −3.20, −4.56.

1-(3-((tert-Butyldimethylsilyl)oxy)benzyl)-8-(4-fluorobenzoyl)-1,3,8-triazaspiro[4.5]dec-2-en-4-one (41). MS (ESI): [M + H]$^+$ = 495.24. Yield: 54%. ^{1}H NMR (400 MHz, acetone-d_6) δ 8.01 (s, 1H), 7.59–7.53 (m, 2H), 7.27–7.21 (m, 2H), 6.95–6.91 (m, 1H), 6.85–6.81 (m, 2H), 4.69–4.65 (m, 2H), 3.49 (s, 2H), 1.92–1.82 (m, 2H), 1.43 (d, J = 7.6 Hz, 2H), 0.97 (s, 9H), 0.20 (s, 6H). ^{13}C NMR (101 MHz, acetone-d_6) δ 184.27, 169.68, 165.44, 162.97, 157.10, 154.05, 139.62, 131.00, 130.65, 130.56, 121.49, 120.49, 120.13, 116.32, 116.11, 44.71, 33.74, 33.39, 26.16, 18.93, −4.14. ^{19}F NMR (376 MHz, acetone-d_6) δ −111.25.

1-(3-Hydroxybenzyl)-8-tosyl-1,3,8-triazaspiro[4.5]dec-2-en-4-one (42). To a solution of derivative **39** in MeOH (5 mL) at 0 °C, a solution of HCl (10% v/v) was dropped slowly until the pH was acidic. The reaction was then allowed to warm to room temperature and stirred for 10 h, monitoring via TLC and MS (ESI). Upon completion of the reaction, the mixture was basified (pH > 9) at 0 °C and the organic solvent was evaporated. The residue was extracted three times with DCM, and the unprotected derivative **42** was obtained as a white solid in 57% yield. MS (ESI): [M + H]$^+$ = 413.14. ^{1}H NMR (400 MHz, chloroform-d) δ 8.02 (s, 1H), 7.68–7.61 (m, 2H), 7.35–7.29 (m, 2H), 7.28–7.17 (m, 2H), 6.83–6.71 (m, 2H), 6.67 (t, J = 2.1 Hz, 1H), 4.59 (s, 2H), 3.73 (dt, J = 12.3, 4.1 Hz, 2H), 2.89–2.79 (m, 2H), 2.42 (s, 3H), 2.18–2.06 (m, 2H), 1.63 (s, 1H). ^{13}C NMR (101 MHz, chloroform-d) δ 156.74, 155.44, 144.16, 136.19, 132.93, 130.85, 129.99, 127.70, 119.92, 116.11, 114.75, 67.65, 45.08, 41.95, 32.07, 21.63.

Synthesis of Intermediates 43 and 44. To a solution of the appropriate compound (**40** and **41**, 1 equiv, 0.61 mmol) in MeOH (5 mL) at 0 °C, $NaBH_4$ (1.3 equiv, 0.78 mmol) was added in small portions. The reaction was allowed to warm to room temperature and stirred for 5 h. After completion of the reaction, as indicated by MS (ESI), the solvent was evaporated, and the residue was resuspended in water and then extracted four times with DCM. The combined organic layers were dried over Na_2SO_4 anhydrous, filtered, and evaporated in vacuum. The crude compound was purified by flash chromatography (1.5:8.5 AcOEt/DCM) to obtain the reduced product as a transparent amorphous compound.

1-(3-((tert-Butyldimethylsilyl)oxy)benzyl)-8-((5-chlorothiophen-2-yl)sulfonyl)-1,3,8-triazaspiro[4.5]decan-4-one (43). MS (ESI): [M + H]$^+$ = 556.14. Yield: 98%. ^{1}H NMR (400 MHz, DMSO-d_6) δ 7.58 (d, J = 4.1 Hz, 1H), 7.38 (d, J = 4.1 Hz, 1H), 7.21 (t, J = 7.8 Hz, 1H), 6.85–6.79 (m, 1H), 6.69 (s, 1H), 4.29 (s, 2H), 4.03 (d, J = 8.5 Hz, 2H), 3.56–3.44 (m, 2H), 3.27 (d, J = 8.6 Hz, 2H), 2.73–2.59 (m, 2H), 1.76 (td, J = 12.7, 12.1, 4.3 Hz, 2H), 1.56 (d, J = 13.5 Hz, 3H), 0.93 (s, 10H), 0.16 (s, 6H). ^{13}C NMR (101 MHz, DMSO-d_6) δ 175.34, 157.61, 155.30, 138.40, 138.01, 135.51, 133.74, 132.97, 129.82, 129.60, 128.79, 120.59, 118.98, 118.85, 118.00, 114.37, 114.25, 60.45, 58.17, 44.21, 44.05, 42.22, 30.46, 25.81, 25.54, 17.93, −3.19, −4.53.

1-(3-((tert-Butyldimethylsilyl)oxy)benzyl)-8-(4-fluorobenzoyl)-1,3,8-triazaspiro[4.5]decan-4-one (44). MS (ESI): [M + H]$^+$ = 497.25. Yield: 57%. ^{1}H NMR (400 MHz, DMSO-d_6) δ 7.53–7.45 (m, 2H), 7.34–7.25 (m, 2H), 7.15–7.09 (m, 1H), 6.70–6.59 (m, 3H), 4.27

(s, 2H), 4.10 (d, J = 8.3 Hz, 2H), 3.40 (t, J = 8.6 Hz, 1H), 1.65 (d, J = 14.2 Hz, 2H), 1.52 (s, 2H), 0.84 (s, 9H), −0.04 (d, J = 0.6 Hz, 5H). ^{13}C NMR (101 MHz, DMSO-d_6) δ 175.53, 168.13, 161.24, 157.65, 138.05, 132.52, 129.58, 129.41, 129.33, 117.90, 115.48, 115.27, 114.32, 114.17, 60.59, 59.59, 44.19, 43.67, 31.52, 25.80, 25.53, 17.79, −3.20.

1-(3-Hydroxybenzyl)-8-tosyl-1,3,8-triazaspiro[4.5]decan-4-one (9). To a solution of compound **42** in MeOH (5 mL) at 0 °C, NaBH$_4$ (1.3 equiv, 0.78 mmol) was added in small portions. The reaction was allowed to warm to room temperature and stirred for 5 h. After completion of the reaction, as indicated by MS (ESI), the solvent was evaporated, and the residue was resuspended in water and then extracted four times with DCM. The combined organic layers were dried over Na$_2$SO$_4$ anhydrous, filtered, and evaporated in vacuum. The crude compound was purified by flash chromatography (1.5:8.5 AcOEt/DCM) to obtain the reduced product as a transparent amorphous in 40% yield. HRMS (ESI): calcd [M + H]$^+$ 416.16385; found 416.16368. Mp: 150−152 °C. HPLC t_R: 24.13 min. ^{1}H NMR (400 MHz, DMSO-d_6) δ 9.45 (s, 1H), 7.67−7.60 (m, 2H), 7.49−7.41 (m, 2H), 7.14−7.07 (m, 1H), 6.64 (ddd, J = 8.1, 2.4, 1.1 Hz, 1H), 6.62−6.57 (m, 2H), 4.22 (s, 2H), 3.97 (d, J = 8.6 Hz, 2H), 3.50 (dt, J = 11.6, 3.8 Hz, 2H), 3.15 (t, J = 8.7 Hz, 1H), 2.46 (d, J = 2.8 Hz, 1H), 2.41 (s, 3H), 1.80−1.69 (m, 2H), 1.52 (d, J = 13.2 Hz, 2H). ^{13}C NMR (101 MHz, DMSO-d_6) δ 175.41, 157.60, 143.56, 138.02, 132.33, 129.84, 129.57, 127.50, 117.97, 114.34, 114.24, 60.40, 58.34, 44.19, 42.09, 30.52, 21.01.

General Procedure for the Synthesis of Compounds 10 and 11. To a solution of the appropriate derivative (**43** and **44**) in MeOH (5 mL) at 0 °C, a solution of HCl (10% v/v) was dropped slowly until the pH was acidic. The reaction was then allowed to warm to room temperature and stirred for 10 h, monitoring via TLC and MS (ESI). Upon completion of the reaction, the mixture was basified (pH > 9) at 0 °C, and the organic solvent was evaporated. The residue was extracted three times with DCM, and the unprotected derivative (**10** and **11**) was obtained as a white solid.

8-((5-Chlorothiophen-2-yl)sulfonyl)-1-(3-hydroxybenzyl)-1,3,8-triazaspiro[4.5]decan-4-one (10). Yield: 87%. Mp: 169−171 °C. HRMS (ESI): calcd [M + H]$^+$ 442.06565; found 442.06517. HPLC t_R: 20.85 min. ^{1}H NMR (400 MHz, DMSO-d_6) δ 9.43 (s, 1H), 7.58 (d, J = 4.1 Hz, 1H), 7.40 (s, 1H), 7.12 (t, J = 7.8 Hz, 1H), 6.69−6.57 (m, 3H), 4.26 (s, 2H), 4.10 (s, 2H), 3.51 (dd, J = 10.0, 6.0 Hz, 2H), 2.74 (d, J = 11.7 Hz, 2H), 1.81 (t, J = 12.3 Hz, 2H), 1.67 (s, 2H). ^{13}C NMR (101 MHz, chloroform-d) δ 156.85, 137.59, 137.24, 134.79, 131.90, 130.34, 127.32, 120.21, 115.54, 114.72, 60.76, 59.59, 45.51, 42.27, 31.37.

8-(4-Fluorobenzoyl)-1-(3-hydroxybenzyl)-1,3,8-triazaspiro[4.5]-decan-4-one (11). MS (ESI): [M + H]$^+$ 383.16. Yield: 67%. HRMS (ESI): calcd [M + H]$^+$ 384.17180; found 384.17812. HPLC t_R: 21.15 min. ^{1}H NMR (400 MHz, acetone-d_6) δ 8.37 (s, 1H), 7.56−7.49 (m, 2H), 7.27−7.19 (m, 2H), 7.17−7.11 (m, 1H), 6.77−6.70 (m, 3H), 4.36 (s, 2H), 4.23 (s, 2H), 3.71 (d, J = 30.4 Hz, 1H), 3.37 (d, J = 39.6 Hz, 2H), 2.99 (s, 1H), 1.86 (d, J = 21.7 Hz, 2H), 1.56 (s, 2H). ^{13}C NMR (101 MHz, acetone-d_6) δ 176.59, 169.38, 162.78, 158.66, 139.51, 134.03, 130.53, 130.43, 130.34, 119.59, 116.14, 115.92, 115.32, 115.29, 61.60, 60.85, 45.40, 32.63, 32.58. ^{19}F NMR (376 MHz, acetone-d_6) δ −113.08.

3-((tert-Butyldimethylsilyl)oxy)benzaldehyde (45). Imidazole (1.2 equiv, 9.83 mmol) was dissolved in DCM (6 mL); next, TBDMSCl (1.2 equiv, 9.83 mmol) and 3-hydroxybenzaldehyde (1 equiv, 8.18 mmol), previously dissolved in DCM (10 mL), were added. This was allowed to react at room temperature for 18 h, monitored by TLC (A0.5P9.5). Afterward, the reaction was quenched by adding deionized H$_2$O, the DCM was evaporated, and the product was extracted in DCM/H$_2$O. After drying and evaporating the solvent, the product of interest was isolated by column chromatography using a petroleum ether/AcOEt (9.5:0.5) eluent mixture. Finally, the organic solvent was evaporated, obtaining a transparent, slightly viscous oil in 83% yield. ^{1}H NMR (400 MHz, chloroform-d) δ 9.95 (s, 1H), 7.47 (dt, J = 7.6, 1.4 Hz, 1H), 7.40 (ddd, J = 8.0, 7.6, 0.4 Hz, 1H), 7.34−7.31 (m, 1H), 7.10 (ddd, J = 8.0, 2.6, 1.2 Hz, 1H), 1.00 (s, 9H), 0.22 (s, 6H).

(3-((tert-Butyldimethylsilyl)oxy)phenyl)methanol (46). Compound **45** (1 equiv, 4 mmol) was dissolved in MeOH (10 mL) and cooled with an ice bath. Then, NaBH$_4$ (1.5 equiv, 6 mmol) was added. This was allowed to react at room temperature for 3 h and monitored via TLC (A0.5P9.5). The reaction was quenched by adding deionized H$_2$O. Subsequently, MeOH was evaporated, the aqueous phase was extracted with DCM, it was dried, and the solvent was evaporated. A colorless oil was obtained in 92% yield. ^{1}H NMR (400 MHz, chloroform-d) δ 7.20 (d, J = 7.8 Hz, 1H), 6.96−6.92 (m, 1H), 6.85 (d, J = 2.1 Hz, 1H), 6.76 (ddd, J = 8.0, 2.5, 1.0 Hz, 1H), 4.64 (s, 2H), 1.65 (s, 1H), 0.99 (d, J = 0.9 Hz, 9H), 0.20 (d, J = 0.9 Hz, 6H).

(3-(Bromomethyl)phenoxy)(tert-butyl)dimethylsilane (47). Compound **46** (1 equiv, 3.64 mmol) was solubilized in anhydrous DCM (15 mL), and PPh$_3$ (1.2 equiv, 4.36 mmol) was added. Then, CBr$_4$ (1.2 equiv, 4.36 mmol) was added in small portions at 0 °C, the ice bath was removed, and it was allowed to react at room temperature for 3 h. The reaction was monitored by TLC (A0.5P9.5). Then, the anhydrous DCM was evaporated to obtain an amorphous oil, and the product of interest was isolated by column chromatography using 100% petroleum ether as the solvent. Finally, the solvent was evaporated, obtaining a colorless oil in 65% yield. ^{1}H NMR (400 MHz, chloroform-d) δ 7.18 (t, J = 7.9 Hz, 1H), 6.97 (dt, J = 7.6, 1.4 Hz, 1H), 6.87 (s, 1H), 6.76 (ddd, J = 8.1, 2.4, 1.0 Hz, 1H), 4.43 (s, 2H), 0.98 (d, J = 0.9 Hz, 10H), 0.20 (s, 6H).

Cells Cultures. HeLa cells were obtained from ATCC and cultured in DMEM medium with phenol red containing 1% penicillin−streptomycin, 10% heat-inactivated fetal bovine serum, and 1% of L-glutamine at 37 °C in 5% CO$_2$.

RPTECs were obtained from ATCC and cultured in renal epithelial cell basal medium from ATCC primary cell solutions enriched with a Renal Epithelial Cell Growth Kit at 37 °C in 5% CO$_2$.

mPTP Activity Assay. Staining solution (160 nM, Incucyte MMP Orange Reagent) was added to the cells (both HeLa and RPTEK) (∼6 × 10^3 cells/well) for 15 min at 37 °C in a 5% CO$_2$ atm. Image acquisitions were performed with a Carl Zeiss microscope at 40×/1.30-N.A. Oligomycin A (1 μM) or drugs (1 μM) were administered 15 min before the beginning of the experiment, while controls remained untreated. To induce mPTP opening, cells were treated with FCCP (20 μM). Imaging was performed for 15 min taking a photo every 5 s.

ImageJ Analysis. ImageJ (NIH) software was used to analyze the pictures. Some regions of interest (ROIs) were selected randomly from the different images. Mean gray values were calculated, and data was exported to Excel. Once the background value was subtracted for each ROI, the resulting data set was normalized. Finally, values were analyzed using the following python libraries: Numpy, Matplotlib, Pandas, Scipy.

Calcein−Cobalt Quenching Assay. HeLa cells were pretreated with either DMSO (Vehicle) or compounds (1 μM) for 15 min and then loaded with calcein acetoxymethyl ester and Co^{2+} as previously described.[28] Staining solution was added to the cells for 15 min at 37 °C in a 5% CO$_2$ atm. Image acquisitions were performed with a motorized Olympus IX81-ZDC inverted microscope with a 40×/1.30-N.A. UPlanFLN oil-immersion objective and Cell MT20E xenon lamp. Ionomycin (1 μM) was administered 30 s after the beginning of the experiment to induce mPTP opening. Values of mPTP activity have been calculated as the slope of the kinetics from ionomycin administration to the first 60 s.

Statistical Analysis. The statistical method included one-way ANOVA with multiple comparisons performed by GraphPad Prism. p values are reported in the figure legends or directly in the figure.

■ ASSOCIATED CONTENT

ⓈI Supporting Information

The Supporting Information is available free of charge at https://pubs.acs.org/doi/10.1021/acs.jmedchem.3c01792.

   Coordinates of the 3D structure of human C ring obtained via homology modeling (PDB)

   Coordinates of the 3D structure of the most representative conformation of compound **6** in complex with human F$_0$ ATP synthase (PDB)

Supplementary methods; general procedures for the preparation of compounds with ^{1}H, ^{13}C, DEPT NMR, HPLC, and HRMS (PDF)

Sequence alignment of human and yeast C subunit of F_0 ATP synthase; docking structure of compound **6** to the human F_O ATP synthase; molecular formula strings for the final compounds **2−11** and their biological assay data (CSV)

■ AUTHOR INFORMATION

Corresponding Authors

Claudio Trapella − *Department of Chemical, Pharmaceutical and Agricultural Sciences, University of Ferrara, 44121 Ferrara, Italy; Laboratory for Technologies of Advanced Therapies (LTTA), 44121 Ferrara, Italy;* ⓘ orcid.org/0000-0002-6666-143X; Email: claudio.trapella@unife.it

Alessandro Arcovito − *Dipartimento di Scienze Biotecnologiche di Base, Cliniche Intensivologiche e Perioperatorie, Università Cattolica del Sacro Cuore, 00168 Roma, Italy; Fondazione Policlinico Universitario "A. Gemelli", IRCCS, 00168 Roma, Italy;* ⓘ orcid.org/0000-0002-8384-4844; Email: alessandro.arcovito@unicatt.it

Authors

Giulia Turrin − *Department of Chemical, Pharmaceutical and Agricultural Sciences, University of Ferrara, 44121 Ferrara, Italy*

Ettore Lo Cascio − *Dipartimento di Scienze Biotecnologiche di Base, Cliniche Intensivologiche e Perioperatorie, Università Cattolica del Sacro Cuore, 00168 Roma, Italy*

Noah Giacon − *Dipartimento di Scienze Biotecnologiche di Base, Cliniche Intensivologiche e Perioperatorie, Università Cattolica del Sacro Cuore, 00168 Roma, Italy*

Anna Fantinati − *Department of Environmental and Prevention Sciences, University of Ferrara, 44121 Ferrara, Italy;* ⓘ orcid.org/0000-0003-0437-5670

Virginia Cristofori − *Department of Chemical, Pharmaceutical and Agricultural Sciences, University of Ferrara, 44121 Ferrara, Italy;* ⓘ orcid.org/0000-0002-6837-6042

Davide Illuminati − *Department of Chemical, Pharmaceutical and Agricultural Sciences, University of Ferrara, 44121 Ferrara, Italy;* ⓘ orcid.org/0000-0002-0321-1941

Delia Preti − *Department of Chemical, Pharmaceutical and Agricultural Sciences, University of Ferrara, 44121 Ferrara, Italy;* ⓘ orcid.org/0000-0002-1075-3781

Giampaolo Morciano − *Department of Medical Sciences, University of Ferrara, 44121 Ferrara, Italy; Laboratory for Technologies of Advanced Therapies (LTTA), 44121 Ferrara, Italy*

Paolo Pinton − *Department of Medical Sciences, University of Ferrara, 44121 Ferrara, Italy; Laboratory for Technologies of Advanced Therapies (LTTA), 44121 Ferrara, Italy;* ⓘ orcid.org/0000-0001-7108-6508

Esther Densu Agyapong − *Department of Medical Sciences, University of Ferrara, 44121 Ferrara, Italy*

Complete contact information is available at:
https://pubs.acs.org/10.1021/acs.jmedchem.3c01792

Author Contributions

§G.T. and E.L.C.: These authors contributed equally.

Author Contributions

The manuscript was written through contributions of all authors. All authors have given approval to the final version of the manuscript.

Notes

The authors declare no competing financial interest.

■ ABBREVIATIONS USED

ATP, adenosine triphosphate; CypD, cyclophilin D; DCM, dichloromethane; DMEM, Dulbecco's modified eagle medium; DMF, dimethylformamide; DMF−DMA, dimethylformamide/dimethylacetal; FCCP, carbonyl cyanide-*p*-trifluoromethoxyphenylhydrazone; HPLC, high-performance liquid chromatography; HTVS, high-throughput virtual screening; I/R, ischemia−reperfusion; IFD, induced fit docking; IMM, inner mitochondrial membrane; IRI, ischemia−reperfusion injury; MD, molecular dynamics; MeOH, methanol; MMPOR, mitochondrial membrane potential Orange Reagent; MPT, mitochondrial permeability transition; mPTP, mitochondrial permeability transition pore; MS/MS, tandem mass spectrometry; PDB, Protein Data Bank; ROI, region of interest; RPTEC, renal proximal tubular epithelial cell; SP, standard precision; THF, tetrahydrofuran; TLC, thin layer chromatography; TMSCN, trimethylsilyl cyanide; XP, extra precision

■ REFERENCES

(1) Meier, P.; Finch, A.; Evan, G. Apoptosis in development. *Nature* **2000**, *407*, 796−801.

(2) Izzo, V.; Bravo-San Pedro, J. M.; Sica, V.; Kroemer, G.; Galluzzi, L. Mitochondrial Permeability Transition: New Findings and Persisting Uncertainties. *Trends in Cell Biology* **2016**, *26*, 655−667.

(3) Halestrap, A. P.; Richardson, A. P. The mitochondrial permeability transition: a current perspective on its identity and role in ischaemia/reperfusion injury. *J. Mol. Cell Cardiol* **2015**, *78*, 129−141.

(4) Halestrap, A. P. A pore way to die: The role of mitochondria in reperfusion injury and cardioprotection. *Biochem. Soc. Trans.* **2010**, *38*, 841−860.

(5) Bonora, M.; Giorgi, C.; Pinton, P. Molecular mechanisms and consequences of mitochondrial permeability transition. *Nat. Rev. Mol. Cell Biol.* **2022**, *23*, 266−285.

(6) Giorgio, V.; et al. Cyclophilin D modulates mitochondrial F0F1-ATP synthase by interacting with the lateral stalk of the complex. *J. Biol. Chem.* **2009**, *284*, 33982−33988.

(7) Algieri, C.; et al. 1,5-disubstituted-1,2,3-triazoles counteract mitochondrial dysfunction acting on F1FO-ATPase in models of cardiovascular diseases. *Pharmacol. Res.* **2023**, *187*, No. 106561.

(8) Roy, S.; et al. Discovery, Synthesis, and Optimization of Diarylisoxazole-3-carboxamides as Potent Inhibitors of the Mitochondrial Permeability Transition Pore. *ChemMedChem.* **2015**, *10*, 1655.

(9) Bonora, M.; et al. Role of the c subunit of the FO ATP synthase in mitochondrial permeability transition. *Cell Cycle* **2013**, *12*, 674−683.

(10) Fantinati, A.; et al. Identification of small-molecule urea derivatives as PTPC modulators targeting the c subunit of F1/Fo-ATP synthase. *Bioorg. Med. Chem. Lett.* **2022**, *72*, No. 128822.

(11) He, J.; et al. Persistence of the mitochondrial permeability transition in the absence of subunit c of human ATP synthase. *Proc. Natl. Acad. Sci. U. S. A.* **2017**, *114*, 3409−3414.

(12) Neginskaya, M. A.; Solesio, M. E.; Berezhnaya, E. V.; Amodeo, G. F.; Mnatsakanyan, N.; Jonas, E. A.; Pavlov, E. V. ATP Synthase C-Subunit-Deficient Mitochondria Have a Small Cyclosporine A-Sensitive Channel, but Lack the Permeability Transition Pore. *Cell Rep.* 2019, *26*, 11−17.e2.

(13) Zhou, W.; Marinelli, F.; Nief, C.; Faraldo-Gómez, J. D. Atomistic simulations indicate the c-subunit ring of the F1Fo ATP synthase is not the mitochondrial permeability transition pore. *eLife* 2017, *6*, e23781.

(14) Alavian, K. N.; et al. An uncoupling channel within the c-subunit ring of the F1F O ATP synthase is the mitochondrial permeability transition pore. *Proc. Natl. Acad. Sci. U. S. A.* 2014, *111*, 10580−10585.

(15) Azarashvili, T.; et al. Potential role of subunit c of F0F1-ATPase and subunit c of storage body in the mitochondrial permeability transition. Effect of the phosphorylation status of subunit c on pore opening. *Cell Calcium* 2014, *55*, 69−77.

(16) Elustondo, P A; Nichols, M; Negoda, A; Thirumaran, A; Zakharian, E; Robertson, G S; Pavlov, E V Mitochondrial permeability transition pore induction is linked to formation of the complex of ATPase C-subunit, polyhydroxybutyrate and inorganic polyphosphate. *Cell Death Discovery* 2016, *2*, 16070.

(17) Morciano, G.; et al. Molecular identity of the mitochondrial permeability transition pore and its role in ischemia-reperfusion injury. *Journal of Molecular and Cellular Cardiology* 2015, *78*, 142−153.

(18) Ferrari, R.; et al. Reperfusion damage — a story of success, failure, and hope —. *Circulation Journal* 2017, *81*, 131−141.

(19) Martin, L. J.; Fancelli, D.; Wong, M.; Niedzwiecki, M.; Ballarini, M.; Plyte, S.; Chang, Q. GNX-4728, a novel small molecule drug inhibitor of mitochondrial permeability transition, is therapeutic in a mouse model of amyotrophic lateral sclerosis. *Front. Cell. Neurosci.* 2014, *8*, 433.

(20) Fancelli, D.; et al. Cinnamic anilides as new mitochondrial permeability transition pore inhibitors endowed with ischemia-reperfusion injury protective effect in vivo. *J. Med. Chem.* 2014, *57*, 5333−5347.

(21) Morciano, G.; et al. Discovery of Novel 1,3,8-Triazaspiro[4.5]-decane Derivatives That Target the c Subunit of F1/FO-Adenosine Triphosphate (ATP) Synthase for the Treatment of Reperfusion Damage in Myocardial Infarction. *J. Med. Chem.* 2018, *61*, 7131−7143.

(22) Symersky, J.; Osowski, D.; Walters, D. E.; Mueller, D. M. Oligomycin frames a common drug-binding site in the ATP synthase. *Proc. Natl. Acad. Sci. U. S. A.* 2012, *109*, 13961−13965.

(23) Bateman, A.; Martin, M.-J.; Orchard, S.; Magrane, M.; Ahmad, S.; Alpi, E.; Bowler-Barnett, E. H; Britto, R.; Bye-A-Jee, H.; Cukura, A.; Denny, P.; Dogan, T.; Ebenezer, T.; Fan, J.; Garmiri, P.; da Costa Gonzales, L. J.; Hatton-Ellis, E.; Hussein, A.; Ignatchenko, A.; Insana, G.; Ishtiaq, R.; Joshi, V.; Jyothi, D.; Kandasaamy, S.; Lock, A.; Luciani, A.; Lugaric, M.; Luo, J.; Lussi, Y.; MacDougall, A.; Madeira, F.; Mahmoudy, M.; Mishra, A.; Moulang, K.; Nightingale, A.; Pundir, S.; Qi, G.; Raj, S.; Raposo, P.; Rice, D. L; Saidi, R.; Santos, R.; Speretta, E.; Stephenson, J.; Totoo, P.; Turner, E.; Tyagi, N.; Vasudev, P.; Warner, K.; Watkins, X.; Zaru, R.; Zellner, H.; Bridge, A. J; Aimo, L.; Argoud-Puy, G.; Auchincloss, A. H; Axelsen, K. B; Bansal, P.; Baratin, D.; Batista Neto, T. M; Blatter, M.-C.; Bolleman, J. T; Boutet, E.; Breuza, L.; Gil, B. C.; Casals-Casas, C.; Echioukh, K. C.; Coudert, E.; Cuche, B.; de Castro, E.; Estreicher, A.; Famiglietti, M. L; Feuermann, M.; Gasteiger, E.; Gaudet, P.; Gehant, S.; Gerritsen, V.; Gos, A.; Gruaz, N.; Hulo, C.; Hyka-Nouspikel, N.; Jungo, F.; Kerhornou, A.; Le Mercier, P.; Lieberherr, D.; Masson, P.; Morgat, A.; Muthukrishnan, V.; Paesano, S.; Pedruzzi, I.; Pilbout, S.; Pourcel, L.; Poux, S.; Pozzato, M.; Pruess, M.; Redaschi, N.; Rivoire, C.; Sigrist, C. J A; Sonesson, K.; Sundaram, S.; Wu, C. H; Arighi, C. N; Arminski, L.; Chen, C.; Chen, Y.; Huang, H.; Laiho, K.; McGarvey, P.; Natale, D. A; Ross, K.; Vinayaka, C R; Wang, Q.; Wang, Y.; Zhang, J. UniProt: the Universal Protein Knowledgebase in 2023. *Nucleic Acids Res.* 2023, *51*, D523−D531.

(24) Sterling, T.; Irwin, J. J. ZINC 15 - Ligand Discovery for Everyone. *J. Chem. Inf. Model.* 2015, *55*, 2324−2337.

(25) Aldrich, C.; et al. The Ecstasy and Agony of Assay Interference Compounds. *J. Med. Chem.* 2017, *60*, 2165−2168.

(26) Friesner, R. A.; et al. Extra precision glide: Docking and scoring incorporating a model of hydrophobic enclosure for protein-ligand complexes. *J. Med. Chem.* 2006, *49*, 6177−6196.

(27) Abraham, M. J.; et al. Gromacs: High performance molecular simulations through multi-level parallelism from laptops to super-computers. *SoftwareX* 2015, *1−2*, 19−25.

(28) Bonora, M.; et al. Comprehensive analysis of mitochondrial permeability transition pore activity in living cells using fluorescence-imaging-based techniques. *Nat. Protoc* 2016, *11*, 1067−1080.

(29) Crompton, M. The mitochondrial permeabitity transition pore and its role in cell death. *Biochem. J.* 1999, *341*, 233−249.

(30) Wacquier, B.; Combettes, L.; Dupont, G. Dual dynamics of mitochondrial permeability transition pore opening. *Sci. Rep.* 2020, *10*, 3924.

(31) Lai, Y.; Zhang, Y.; Zhou, S.; Xu, J.; Du, Z.; Feng, Z.; Yu, L.; Zhao, Z.; Wang, W.; Tang, Y.; Yang, X.; Guddat, L. W.; Liu, F.; Gao, Y.; Rao, Z.; Gong, H. Structure of the human ATP synthase. *Mol. Cell* 2023, *83*, 2137−2147.e4.

(32) Pedriali, G.; Ramaccini, D.; Bouhamida, E.; Branchini, A.; Turrin, G.; Tonet, E.; Scala, A.; Paterngnani, S.; Pinotti, M.; Trapella, C.; Giorgi, C.; Tremoli, E.; Campo, G.; Morciano, G.; Pinton, P. 1,3,8-Triazaspiro[4.5]decane Derivatives Inhibit Permeability Transition Pores through a FO-ATP Synthase c Subunit Glu119-Independent Mechanism That Prevents Oligomycin A-Related Side Effects. *Int. J. Mol. Sci.* 2023, *24*, 6191.

(33) Dixon, S. L.; et al. PHASE: A new engine for pharmacophore perception, 3D QSAR model development, and 3D database screening: 1. Methodology and preliminary results. *J. Comput. Aided Mol. Des* 2006, *20*, 647−671.

(34) Madhavi Sastry, G.; Adzhigirey, M.; Day, T.; Annabhimoju, R.; Sherman, W. Protein and ligand preparation: Parameters, protocols, and influence on virtual screening enrichments. *J. Comput. Aided Mol. Des* 2013, *27*, 221−234.

(35) Sherman, W.; Beard, H. S.; Farid, R. Use of an induced fit receptor structure in virtual screening. *Chemical Biology and Drug Design* 2006, *67*, 83−84.

(36) Sherman, W.; Day, T.; Jacobson, M. P.; Friesner, R. A.; Farid, R. Novel procedure for modeling ligand/receptor induced fit effects. *J. Med. Chem.* 2006, *49*, 534−553.

(37) Greenwood, J. R.; Calkins, D.; Sullivan, A. P.; Shelley, J. C. Towards the comprehensive, rapid, and accurate prediction of the favorable tautomeric states of drug-like molecules in aqueous solution. *Journal of Computer-Aided Molecular Design* 2010, *24*, 591−604.

(38) Lee, J.; et al. CHARMM-GUI Input Generator for NAMD, GROMACS, AMBER, OpenMM, and CHARMM/OpenMM Simulations Using the CHARMM36 Additive Force Field. *J. Chem. Theory Comput* 2016, *12*, 405−413.

(39) Guterres, H.; Park, S.-J.; Zhang, H.; Perone, T.; Kim, J.; Im, W. CHARMM-GUI: high-throughput simulator for efficient evaluation of protein−ligand interactions with different force fields. *Protein Sci.* 2022, *31*, No. e4413.

(40) Huang, J.; et al. CHARMM36m: An improved force field for folded and intrinsically disordered proteins. *Nat. Methods* 2017, *14*, 71−73.

(41) Khan, H. M.; MacKerell, A. D.; Reuter, N. Cation-π Interactions between Methylated Ammonium Groups and Tryptophan in the CHARMM36 Additive Force Field. *J. Chem. Theory Comput* 2019, *15*, 7−12.

(42) Michaud-Agrawal, N.; Denning, E. J.; Woolf, T. B.; Beckstein, O. MDAnalysis: A toolkit for the analysis of molecular dynamics simulations. *J. Comput. Chem.* 2011, *32*, 2319−2327.

(43) Adasme, M. F.; et al. PLIP 2021: Expanding the scope of the protein-ligand interaction profiler to DNA and RNA. *Nucleic Acids Res.* 2021, *49*, W530−W534.